ISSN 2410-3454

Journal of Engineering Applications

Volume 10, Issue 29 – January – June – 2023

ECORFAN®

Journal of Engineering Applications, Volume 10, Issue 29, June, 2023, is a journal published biannually by ECORFAN - Bolivia. 21 Santa Lucía, CP-5220. Libertadores - Sucre - Bolivia. WEB: www.ecorfan.org, revista@ecorfan.org. Editor in Chief: JALIRI-CASTELLON, María Carla Konradis. PhD. ISSN-2410-3454. Responsible for the last update of this issue of the ECORFAN Informatics Unit. ESCAMILLA-BOUCHÁN, Imelda. PhD, LUNA-SOTO, Vladimir. PhD. Updated as of June 30, 2023.

Journal of Engineering Applications

Definition of Journal

Scientific Objectives

Support the international scientific community in its written production Science, Technology and Innovation in the Field of Engineering and Technology, in Subdisciplines of civil engineering, systems engineering, telecommunications engineering, electronic engineering, energy engineering, hydraulic engineering, industrial engineering, mechanical engineering, engineering, geological metallurgical, mining engineering, naval engineering, nuclear engineering, petroleum and petrochemical engineering, chemical engineering.

ECORFAN-Mexico SC is a Scientific and Technological Company in contribution to the Human Resource training focused on the continuity in the critical analysis of International Research and is attached to CONACYT-RENIECYT number 1702902, its commitment is to disseminate research and contributions of the International Scientific Community, academic institutions, agencies and entities of the public and private sectors and contribute to the linking of researchers who carry out scientific activities, technological developments and training of specialized human resources with governments, companies and social organizations.

Encourage the interlocution of the International Scientific Community with other Study Centers in Mexico and abroad and promote a wide incorporation of academics, specialists and researchers to the publication in Science Structures of Autonomous Universities - State Public Universities - Federal IES - Polytechnic Universities - Technological Universities - Federal Technological Institutes - Normal Schools - Decentralized Technological Institutes - Intercultural Universities - S & T Councils - CONACYT Research Centers.

Scope, Coverage and Audience

Journal of Engineering Applications is a Journal edited by ECORFAN-Mexico S.C in its Holding with repository in Bolivia, is a scientific publication arbitrated and indexed with semester periods. It supports a wide range of contents that are evaluated by academic peers by the Double-Blind method, around subjects related to the theory and practice of civil engineering, systems engineering, telecommunications engineering, electronic engineering, energy engineering, hydraulic engineering, industrial engineering, mechanical engineering, engineering, geological metallurgical, mining engineering, naval engineering, nuclear engineering, petroleum and petrochemical engineering, chemical engineering with diverse approaches and perspectives, that contribute to the diffusion of the development of Science Technology and Innovation that allow the arguments related to the decision making and influence in the formulation of international policies in the Field of Engineering and Technology. The editorial horizon of ECORFAN-Mexico® extends beyond the academy and integrates other segments of research and analysis outside the scope, as long as they meet the requirements of rigorous argumentative and scientific, as well as addressing issues of general and current interest of the International Scientific Society.

Editorial Board

Arbitration Committee

Assignment of Rights

The sending of an Article to Journal of Engineering Applications emanates the commitment of the author not to submit it simultaneously to the consideration of other series publications for it must complement the Originality Format for its Article.

The authors sign the Authorization Format for their Article to be disseminated by means that ECORFAN-Mexico, S.C. In its Holding Bolivia considers pertinent for disclosure and diffusion of its Article its Rights of Work.

Declaration of Authorship

Indicate the Name of Author and Coauthors at most in the participation of the Article and indicate in extensive the Institutional Affiliation indicating the Department.

Identify the Name of Author and Coauthors at most with the CVU Scholarship Number-PNPC or SNI-CONACYT- Indicating the Researcher Level and their Google Scholar Profile to verify their Citation Level and H index.

Identify the Name of Author and Coauthors at most in the Science and Technology Profiles widely accepted by the International Scientific Community ORC ID - Researcher ID Thomson - arXiv Author ID - PubMed Author ID - Open ID respectively.

Indicate the contact for correspondence to the Author (Mail and Telephone) and indicate the Researcher who contributes as the first Author of the Article.

Plagiarism Detection

All Articles will be tested by plagiarism software PLAGSCAN if a plagiarism level is detected Positive will not be sent to arbitration and will be rescinded of the reception of the Article notifying the Authors responsible, claiming that academic plagiarism is criminalized in the Penal Code.

Arbitration Process

All Articles will be evaluated by academic peers by the Double Blind method, the Arbitration Approval is a requirement for the Editorial Board to make a final decision that will be final in all cases. MARVID® is a derivative brand of ECORFAN® specialized in providing the expert evaluators all of them with Doctorate degree and distinction of International Researchers in the respective Councils of Science and Technology the counterpart of CONACYT for the chapters of America-Europe-Asia- Africa and Oceania. The identification of the authorship should only appear on a first removable page, in order to ensure that the Arbitration process is anonymous and covers the following stages: Identification of the Journal with its author occupation rate - Identification of Authors and Coauthors - Detection of plagiarism PLAGSCAN - Review of Formats of Authorization and Originality-Allocation to the Editorial Board-Allocation of the pair of Expert Arbitrators-Notification of Arbitration -Declaration of observations to the Author-Verification of Article Modified for Editing-Publication.

Instructions for Scientific, Technological and Innovation Publication

Knowledge Area

The works must be unpublished and refer to topics of civil engineering, systems engineering, telecommunications engineering, electronic engineering, energy engineering, hydraulic engineering, industrial engineering, mechanical engineering, engineering, geological metallurgical, mining engineering, naval engineering, nuclear engineering, petroleum and petrochemical engineering, chemical engineering and other topics related to Engineering and Technology

Presentation of the content

In the first article we present, *Experimental and numerical calibration in a critical flow venturi of close to sonic flow*, by RIVERA-LÓEPZ, Jesús Eduardo, ARCINIEGA-MARTÍNEZ, José Luis, LÓPEZ-AGUADO-MONTES, José Luis and GUTIERREZ-PAREDES, Guadalupe Juliana, with secondment at Instituto Politécnico Nacional; as a second article we present, *Development of prototype and measurement, control and automation system in real time for small production greenhouses*, by MUÑOZ-FLORES, Cristofer Alexis, SOTO-MORALES, Emilia Itzel, HERRERA-DIAZ, Israel Enrique and GAMIÑO-RAMIREZ, Edith Alejandra, with secondment at Universidad de Guanajuato; as third article we present, *Improvement of the efficiency in the injection process in a company of the automotive sector through the implementation of the SMED (Single-Minute Exchange of Die) methodology*, by VÁZQUEZ-ROSAS Sergio, HERNÁNDEZ-SÁNCHEZ Uriel Alejandro, CABALLERO-LÓPEZ Emma Isabel and VALLEJO-HERNANDEZ Arely, with secondment at Universidad Tecnológica del Centro de Veracruz; as final article we present *Determination of risk zones by thermal flow, generated by BLEVE to a tank with LP gas, using mathematical models and ALOHA® software*, by TORRES-VALLE, José Bernardo, HERNÁNDEZ-BORJA, Carlos, PEZA-ORTÍZ, Edebaldo and PÉREZ-GALINDO, Liliana Eloisa, with secondment at Universidad Tecnológica Fidel Velázquez.

Content

Article **Journal of Engineering Applications**

June 2023, Vol.10 No.29 1-12

Experimental and numerical calibration in a critical flow venturi of close to sonic flow

Calibración experimental y numérica de flujo cercano al sónico en un Venturi de flujo critico

RIVERA-LÓEPZ, Jesús Eduardo*†, ARCINIEGA-MARTÍNEZ, José Luis, LÓPEZ-AGUADO-MONTES, José Luis and GUTIERREZ-PAREDES, Guadalupe Juliana

Instituto Politécnico Nacional, Escuela Superior de Ingeniería Mecánica y Eléctrica Unidad Azcapotzalco, México.

ID 1st Author: *Jesús Eduardo, Rivera-López* / **ORC ID:** 0000-0003-3988-9305, **CVU CONAHCYT ID:** 161653

ID 1st Co-author: *José Luis, Arciniega-Martínez* / **ORC ID:** 0000-0003-4996-8146, **CVU CONAHCYT ID:** 161637

ID 2nd Co-author: *José Luis, López-Aguado-Montes* / **ORC ID:** 0009-0009-6322-4937, **CVU CONAHCYT ID:** 229257

ID 3rd Co-author: *Guadalupe Juliana, Gutierrez-Paredes* / **ORC ID:** 0000-0003-2918-7377, **CVU CONAHCYT ID:** 122745

DOI: 10.35429/JEA.2023.29.10.1.12 Received: January 10, 2023; Accepted: June 30, 2023

Abstract

This work introduces a new study in discharge coefficient performance in ***CFV*** when the throat flow is close to sonic regime ***Ma*** ≈ 1 and the throat strangulation is not fully developed. Thus, two ***CFV*** of 0,56 and 2,24 mm diameter were experimentally calibrated by applying the volume averaging method; experimental calibration allowed to estimate C_d and measure uncertainty, for 2,24 mm diameter C_d is 7,34% higher than for 0,56 mm diameter when Ma global is 7,30 % higher. Based on experimental calibration results and ***CFV*** geometries, numerical experiments were realized to explain how ***Ma*** ≈ 1 flow deviates C_d from the theoretical value, concluding compressibility affects thickness scrolling relation since it is 35,92% smaller for 2,24 mm diameter than 0,56 mm, giving a better approximation for C_d to the theoretical value for this throat diameter. Finally, numerical C_d models were obtained to evaluate the deviation these flow conditions produce in respect of empirical and numerical models, finding the numerical model's maximum error is 6,68% and the empirical model's maximum error is 1,64% under identical stagnation conditions.

Critical flow venturi, Sonic flow, Experimental calibration

Resumen

Este trabajo presenta un nuevo estudio del comportamiento del coeficiente de descarga en ***CFV*** cuando el flujo en la garganta está próximo al régimen sónico ***Ma*** ≈ 1 y la estrangulación en la garganta no se alcanzó por completo. Para ello, se calibro experimentalmente dos ***CFV*** de 0,56 y 2,24 mm de diámetro de garganta por el método de acumulación de volumen; con la calibración experimental se estimó el C_d y la incertidumbre de la medición, encontrando que el diámetro de garganta de 2,24 mm es 7,34 % más alto respecto a 0,56 mm cuando el Ma global es 7,30 % más elevado. Con los resultados de la calibración experimental y con la geometría de los ***CFV*** se realizaron experimentos numéricos con el objetico de explicar como el flujo Ma ≈ 1 desvía al C_d del valor teórico, encontrando que la compresibilidad afecta la relación del espesor de desplazamiento δ^*/d, ya que es 35,92 % más pequeño para el diámetro de 2,24 mm en comparación de 0,56 mm, provocando que el C_d tenga una mejor aproximación al valor teórico para este diámetro de garganta. Finalmente se obtuvieron modelos numéricos del C_d para cada diámetro de garganta con el objetivo de tener una forma de evaluar la desviación que produce estas condiciones de flujo con respecto a modelos empíricos y numéricos, encontrando que los modelos numéricos tienen un error máximo de 6,68 % y los modelos empíricos el error máximo es de 1,64 % en condiciones de estancamiento iguales.

Venturi de flujo crítico, Flujo sónico, Calibración experimental

Citation: RIVERA-LÓEPZ, Jesús Eduardo, ARCINIEGA-MARTÍNEZ, José Luis, LÓPEZ-AGUADO-MONTES, José Luis and GUTIERREZ-PAREDES, Guadalupe Juliana. Experimental and numerical calibration in a critical flow venturi of close to sonic flow. Journal of Engineering Applications. 2023. 10-29:1-12.

* Correspondence of the Author (E-mail: jriveral@ipn.mx)
† Researcher contributing as first author.

Article **Journal of Engineering Applications**
June 2023, Vol.10 No.29 1-12

Introduction

In vapor generation in the electrical industry, natural gas plays an important role in the replacement of coal and fuel oil, since it is a cheaper fuel and has more calorific power, talking about energy supplied. It implies vapor generation cost reduces to 80% by using natural gas. Traditionally, subsonic devices have been used ($Ma \leq 0,3$) to measure natural gas flow. However, these low uncertainty devices 0,3 to 3,0% [10] lose millions of dollars because of measuring uncertainty. Consequently, metrology laboratories and research centers have developed investigations on critical flow measure elements ($Ma = 1$). These measure devices are known as Critical Flow Venturi (***CFV***), where the uncertainty range for these devices goes between 0,03 and 0,3 [10]. This inherent property makes them a superior measure device compared to subsonic measure devices. The ***CFV***s are calibrated by using air and applied in natural gas measure, their performance range oscillates from 10 to 300 m^3/h, with pressures to 700 kPa [14]. Measure quality depends directly on the discharge coefficient magnitude, C_d, which comprises every irreversibility on gas flow measure and ***CFV*** geometry. Some irreversibilities causing derivation of C_d from the theoretical value are, for example, viscous diffusivity, compressibility effects, thermal boundary layer [12], hydrodynamics' boundary layer thickness, entrance geometry, rugosity, humidity, chemical gas composition, etc. The research spectrum to understand and improve deviation mechanisms from theoretical value is extremely wide, for example, Chunhui [4] focused his study on how throat diameter affects flow characteristics, he measured a discharge coefficient of 21 super ***CFV*** in a flow range from 2,39 X 10^4 to 2,8 X 10^6 ***Re***, obtaining C_d can variate to 2,3% for identical throat diameters under different stagnation pressures, concluding to have precise C_d values, similar calibration stagnation pressures are required. Jae Hyung Kim [11] realized another computational study focused on geometry effects on C_d, where he variated the diffuser angle from 2 to 8° and throat diameter from 0,2 to 5 mm, where it was found for throat diameters less than 2 mm the diffusor angle affects C_d considerably and it would be affected the most as less as the throat diameter is, this because of sonics line ubication, which is more significant for smaller diameters.

Junji Nagao [13] realized numerical research about state effects equations on C_d by using H_2 as a working fluid, where Redliche-Kwon and Lee-Kesler equations have good behavior on C_d at high ***Re***, but also C_d decreases while ***Re*** increases when 1,0 X 10^5 < ***Re*** < 2,8 X 10^6. On the other hand, Ishibashi [15] developed a theoretical model from Hall's equation in the viscous zone and Geropp's equation about the boundary layer, he verified his model by the calibration of 25 super ***CFV***s, resulting for ***Re*** > 8 X 10^4 theoretical and experimental coefficients' difference is 0,04%. Aaron [2] used dimensional metrology to measure curvature and throat diameter for nine ***CFV***s, by throat curvature and Stratford-Kliegel and Gerrop-Kliegel theoretical C_d models he determined a C_d theoretical model for laminar, transition, and turbulent flow, in a range from 7,2 X 10^4 to 2,5 X 10^6 ***Re***, where diameter and throat curvature corrections realized to theoretical models show good results since deviation respect to experimental coefficient is less than 0,017 and 0,07% for turbulent and laminar flow respectively. Ishibashi [7] in transition flow, studied C_d dependence on concerning curvature, entrance diameter, and diffusor longitude, to do this, he designed ten super ***CFV***s, finding an empirical C_d equation that involves the whole ISO 9300 flow regimen. The experimental results were compared with the Stratford equation and Hall-Geropp combined equation, concluding Geropp's equation is precise enough, which does not happen with Hall and Stratford's when the entrance curvature is small. Mickan [3] presents the C_d numerical calculus based on laminar and turbulent boundary layer integral methods, the results were compared with experimental measures on laminar and turbulent regimes, verifying good quality in numerical results. Critical and sonic flow in Venturi nozzles gas flow measure is the throat flow necessary condition for the approximation of discharge coefficient to unity, hence sonic nozzles work in the turbulent and sonic range. For this reason, investigations are focused on solving the inherent problems at this flow condition, that's why the present work objective is to study the compressibility and flow regime effects on C_d when the throat's strangulation isn't fully developed $Ma \approx 1$ in an experimental and numerical way.

ISSN: 2410-3454

Operating principle of convergent-divergent sections

When a compressible flow flows through a convergent-divergent section, gas velocity reaches a maximum value in the minimum surface point (nozzle's throat), and the throat velocity fluid increases in function of an upstream and downstream pressure difference, this velocity limit value is the sound velocity or critical condition [5;19]. Under this condition, the Venturi nozzle is blocked or strangled, given that the block is a physical restriction caused by critical flow, the maximum mass flow rate that flows in the throat Venturi nozzle is given in this condition. In a dimensionless flow with negligible viscosity, theoretically, a relation can be used to predict critical Venturi nozzle metrological behavior, and, using this approximation, it can be demonstrated an ideal flow across a nozzle is governed by the following equation [17].

$$\dot{m}_{ideal} = \frac{P_0 A^* C^*}{\sqrt{R_{gas} T_0}} \quad (1)$$

This analytical model assumes that flow across the Venturi nozzle presents critical flow characteristics (***Ma*** = 1). According to CODATA 2018, the universal gas constant is equal to ***Ru*** = 8.314 462 618 [J mol-1 K-1]. From Pitchard [1] molecular air mass is equal to 28,96546 kg/kmol.

If required a better estimation of mass rate, it's recommended to experimentally calibrate the Venturi nozzle, when the Venturi's discharge coefficient is a supplement of the ideal flow considerations, equation (1).

The discharge coefficient C_d [5] is defined as:

$$C_d = \frac{\dot{m}_{real}}{\dot{m}_{theorical}} \quad (2)$$

Aaron [2] defined the discharge coefficient as always less than unity, this condition assumes C_d calculation by using the real throat diameter, and the mass flow rate is not affected by vibrational relaxation. For a given Venturi nozzle geometry, the discharge coefficient variates as a function of flow relation through the same, and most frequently this function is expressed in Reynolds number terms defined by John D. Wright [21]:

$$Re = \frac{4\dot{m}_{real}}{\pi d \mu_0} \quad (3)$$

$$\mu_0 = \left(\frac{145{,}8\ T_0^{1,5}}{110{,}4 + T_0}\right) \quad (4)$$

Where: μ_0 – units are Pa·s and T_0 is Kelvin.

Calculation of the discharge coefficient "C_d"

The methodology provided by Standard ISO-9300, for mass flow rate calculation through a critical Venturi nozzle, includes the following restrictions:

- Isentropic flow.
- Dimensionless flow.
- Perfectly calorific gas fluid.

Equations (1, 2 y 3) are completed with the restrictions presented before and the following expressions:

Critical flow coefficient ***C**** involves thermodynamic changes in the isentropic flow of the nozzle throat under stagnation conditions. In real gas applications, ***C**** depends on pressure, temperature, and chemical gas composition [21].

$$C^* = 0{,}68309 + 1{,}42025X10^{-5}T_0 - 2{,}80046X10^{-5}T_0 + 3{,}47447X10^{-5}P_0 - 1{,}80997X10^{-7}P_0T_0 + 2{,}46278X10^{-10}P_0 \quad (5)$$

Where: P_0- is given in kPa, T_0 - in Kelvin.

If compressibility effects in the Venturi's throat want to be known, Mach dimensionless number must be used:

$$Ma = \frac{V}{C} \quad (6)$$

Where, environment's velocity ***V*** is determined by the mass flow rate, the throat diameter ***d***, and the stagnation density ρ_0; stagnation density is determined by the state equation of perfect gasses.

$$V = \frac{4\dot{m}}{\pi d^2 \rho_0} \quad (7)$$

The sound velocity ***c*** in the throat is determined by the stagnation temperature T_0, thus:

$$c = \sqrt{\gamma R_{gas} T_0} \quad (8)$$

ISSN: 2410-3454

Substituting equations 7 and 8 in 6, an expression to estimate the ***Ma*** number is obtained.

$$Ma = \frac{4\dot{m}\sqrt{T_0 R_{gas}}}{\pi d^2 P_0 \gamma^{1/2}} \quad (9)$$

Flow is given in kg/s, $\boldsymbol{d}$ en meters, $\boldsymbol{\rho_0}$ in kg/m^3, $\boldsymbol{\gamma}$ is the specific heat relation, $\boldsymbol{R_{gas}}$ – is expressed in J/kg·K, $\boldsymbol{T_0}$ – in Kelvin.

Specific heat relation, $\boldsymbol{\gamma}$, can be determined by [21]:

$$C^* = 0{,}68309 + 1{,}42025X10^{-5}T_0 - 2{,}80046X10^{-5}T_0 + 3{,}47447X10^{-5}P_0 - 1{,}80997X10^{-7}P_0T_0 + 2{,}46278X10^{-10}P_0 \quad (10)$$

Where, $\boldsymbol{P_0}$ is given in kPa and $\boldsymbol{T_0}$ - in Kelvin. Finally, the discharge coefficient $\boldsymbol{C_d}$ [21], is estimated by the following equation:

$$C_d = \frac{4\dot{m}\sqrt{R_{gas}T_0}}{\pi d^2 C^* P_0} \quad 11)$$

Experimental calibration and estimation of uncertainty

Venturi nozzles used in this work are from Flow System© with throat diameters of 0,088 in (2,24 mm) and 0,022 in (0,56 mm). The calibration patron used is based on a quantity of volume recollection in a lapse of time, the volumetric flow rate in charge of moving the piston or bell is calculated by the pulses and recollection time, the equation that allows to calculate the flow through the patrons is the following:

$$Q = \frac{C \cdot 60}{Kt} \quad (12)$$

Where $\boldsymbol{K}$ is a constant equal to 543,2 pulses/L for the bell's patron and 13655,8 pulses/L for the piston, $\boldsymbol{C}$ is the number of pulses and t is the recollection time [16]. The mass flow rate will be estimated by multiplying equation twelve by the density of gas in the bell or piston. In air density measure floatability correction in wet air is currently the biggest part of uncertainty [1]. Besides, humidity in air causes deviation in the ideal behavior of thermodynamic properties of the fluid [9], thus, to use the equations presented before, calibration will be realized under the flow condition $\boldsymbol{HR} \approx 0$, therefore calculation of $\boldsymbol{\rho}$, $\boldsymbol{\gamma}$ and $\boldsymbol{*C}$, will be under dry air conditions, then equations 5, 10, and 13 are valid. Density is calculated by [21]:

$$\rho = \frac{1}{1{,}23838 + 287{,}04\frac{T_P}{P_P} - 30122T_P^{-1{,}334}} + \frac{1}{-7{,}3049X10^{-4}\frac{P_P}{T_P} + 2{,}5304X10^{-2}\frac{P_P}{T_P^{1{,}25}}} \quad (13)$$

Where density is given in g/cm^3, $\boldsymbol{P_P}$ units are kPa and $\boldsymbol{T_P}$ are Kelvin. From equations 12 and 13 mass flow rate is calculated, equation 14.

$$\dot{m} = \frac{C \cdot 60}{Kt}\rho \quad (14)$$

To find uncertainty is suggested to use the law of propagation uncertainty [6;20], equation 15.

$$u_C^2 = \sum_{i=1}^{N}\left(\frac{\partial f}{\partial x_i}\right)^2 u_{x_i}^2 \quad (15)$$

Where $\boldsymbol{f} = \boldsymbol{f(x_1, x_2, x_3 \ldots\ldots\ldots\ldots\ldots x_n)}$ then $\boldsymbol{u(f)}$ is given by equation 15.

CENAM expressed their measures with a trust level not less than 95% ($\boldsymbol{p}$ = 95,45 %) [20], the purpose is to have a coverage factor $\boldsymbol{k}$ = 2,00 on normal distribution limit, therefore, all calculations realized in this work will have this coverage level. Calibration points between venturi nozzles are the pressures $\boldsymbol{P}$ of 200, 300, 400, 500 y 600 kPa, having a barometric pressure $\boldsymbol{P_b}$ = 80365 Pa. Tables 1 and 2 show average data measured of six realized repetitions for each calibration point for both critical flow Venturi nozzles.

P (kPa)	T (K)	P_p (kPa)	T_p (K)	C (pulses)	t(s)
200,83	294,21	80,78	293,93	60187,00	40,77
300,40	294,21	80,79	293,94	60313,50	27,14
400,67	294,18	80,81	293,96	60637,50	20,39
500,09	294,55	80,82	293,03	60739,67	16,33
601,25	294,59	80,83	293,02	60,741,83	13,62

Table 1 Experimental average data measured, d = 0,56 mm
Source: Own elaborated

P (kPa)	T (K)	P_p (kPa)	T_p (K)	C (pulses)	T (s)
200,48	293,04	80,91	293,17	60217,33	59,51
300,49	293,17	80,92	293,16	60386,33	39,58
400,46	293,29	80,93	293,16	60460,50	29,67
500,44	293,39	80,94	293,17	60607,67	23,85
600,83	293,36	80,95	293,20	60238,50	19,66

Table 2 Experimental average data measured, d = 2,24 mm
Source: Own elaborated

ISSN: 2410-3454

Using experimental data from Tables 1 and 2 as well as equations 12, 13 and 14, volumetric flow rate ***Q***, density, ***ρ***, and mass flow rate, $\dot{m}$, are going to be calculated.

With mass flow rate estimation and using stagnation enthalpy concept for an ideal gas and an isentropic stationary flow [19], stagnation pressure, P_0, and temperature, T_0, can be determined in the entrance of the Venturi:

$$T_0 = T_1 + \frac{{}^1/_2 V_1^2}{C_p} \tag{16}$$

The condition belongs to the Venturi entrance measures, P_0 y T_0. From continuity and state equation, the following equations are obtained:

$$V_1 = \frac{4\dot{m}}{\rho_1 \pi d_1^2} \tag{17}$$

$$\rho_1 = \frac{P_1}{R_{gas} T_1} \tag{18}$$

Substituting equations 17 and 18 in 16:

$$T_0 = T_1 + \frac{1}{2C_p}\left(\frac{4\dot{m}R_{gas}T_1}{\pi d^2 P_1}\right)^2 \tag{19}$$

Mach number (air) in the Venturi entrance is calculated using the result of equation 19 [18]:

$$Ma = 5\left[\frac{T_0}{T_1} - 1\right] \tag{20}$$

Stagnation pressure is determined by using equation 20 result:

$$P_0 = P_1[1 + 0{,}2Ma^2]^{3.5} \tag{21}$$

Results of equations 19 and 21 are used to calculate critical flow factor ***C**** and discharge coefficient C_d, equations 5 and 11. Following the procedure described in section 3, uncertainty in measures is determined, in Tables 3 and 4.

$\dot{m}$ (kg/s)	P_o (kPa)	T_0 (K)	C*	C_d	u_{Cd} (%)
0,00010	201,32	294,41	0,6878	0,8881	0,026
0,00016	301,29	294,46	0,6881	0,8934	0,021
0,00021	402,00	294,46	0,6884	0,8964	0,020
0,00026	501,89	294,85	0,6887	0,8984	0,019
0,00031	603,01	294,90	0,6889	0,8954	0,020

Table 3 Calibration results, d= 0,56 mm
Source: Own elaborated

$\dot{m}$ (kg/s)	P_o (kPa)	T_0 (K)	C*	C_d	u_{Cd} (%)
0,00179	201,05	293,28	0,6878	0,9605	0,031
0,00270	301,54	293,46	0,6881	0,9662	0,027
0,00361	402,02	293,61	0,6884	0,9682	0,026
0,00450	502,53	293,74	0,6887	0,9663	0,028
0,00543	603,48	293,73	0,6889	0,9696	0,030

Table 4 Calibration results, d = 2,24 mm
Source: own elaborated

By Reynolds (***Re***) and Mach (***Ma***) dimensionless numbers, calibration results are graphed, to calculate these dimensionless numbers, equations 3, 4, 9, and 10 are used. The results are shown in Tables 5 and 6.

μ_0 (Pa·s)	γ	Re	Ma
0,000127	1,42	1853,06	0,890
0,000127	1,42	2789,69	0,895
0,000127	1,42	3735,07	0,898
0,000127	1,42	4666,57	0,901
0,000127	1,42	5596,66	0,899

Table 5 Calculation of μ_0, ɣ, Re y Ma, Venturi nozzle d = 0,56 mm
Source: own elaborated.

μ_0 (Pa·s)	γ	Re	Ma
0,000127	1,40	8042,42	0,962
0,000127	1,41	12124,95	0,968
0,000127	1,41	16190,18	0,970
0,000127	1,41	20190,60	0,968
0,000127	1,41	24338,66	0,972

Table 6 Calculation of μ_0, ɣ, Re y Ma, Venturi nozzle d = 2,24 mm
Source: own elaborated

Analysis of results

According to the results obtained, discharge coefficients for both Venturi nozzles increase in function of flow regime, Figure 1, uncertainty associated in each calibration point is shown in Tables 3 and 4, from this, estimated uncertainty in the stabled limits by [10]. Comparing obtained results with Chunhui's shown uncertainty estimation is close to values reported by [4], which proves good measure practice and accurate procedure of uncertainty estimation developed in this calibration.

Aaron [2] reported ***CFV*** calibration in laminar, transition, and turbulent flow, $7.2 \times 10^4 \leq Re \leq 2.5 \times 10^6$, from this it can be determined for both Venturi nozzles calibration was realized in laminar and turbulent flow, see Graphs 1 and 2.

ISSN: 2410-3454

Dispersion in Graph 2 shows the linear data adjust, the adjusted result are empirical equations 22 and 23 for Venturi nozzles of 0,56 and 2,24 mm respectively, which will be discussed later.

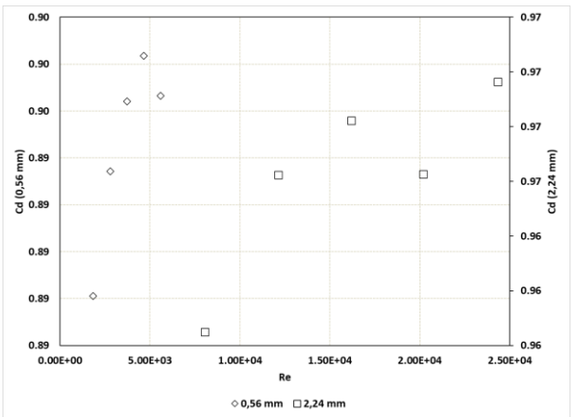

Graphic 1 Calibration results, C_d vs Re, 0,56 y 2,24 mm
Source: Own elaborated

In both Venturi nozzles, the Flow regime is totally viscous, and this way, the relation $1/\boldsymbol{Re}^{0,5}$ increases because the flow regime decreases, and $\boldsymbol{C_d}$ decreases linearly. The prevalence of viscous forces produces the deviation of real flow in respect of theoretical value from equation one, as said by Cruz-Maya [8], for this reason, high viscous shear stress in the boundary layer leads to a maximum area on the throat having as result that the throat's flow won't be the maximum as theory indicates for adiabatic-isentropic flow in divergent-convergent sections [5;19] and, therefore, it will directly and irreversibly affect the $\boldsymbol{C_d}$ magnitude from the ideal value. In addition, $\boldsymbol{C_d}$ magnitude also depends on flow compressibility, ***Ma***; the effective area in the throat when sonic flow is achieved ***Ma***=1, under this flow condition, small variations of static pressure through the transversal plane in the throat won't have any important effect on mass flow rate $\boldsymbol{\partial\rho\forall/\partial P}$ [18], therefore, mass flow rate will be constant because static pressure keeps boundary layer thickness reduced to its minimum value, $\boldsymbol{\delta(x)_{min}}$. In the boundary layer thickness $\boldsymbol{\delta(x)}$ flow is supersonic ***Ma*** > 1 and outside the boundary layer the flow is subsonic ***Ma*** < 1[8]. In figure 3 subsonic flow is shown, the 0,56 mm Venturi nozzle is further from sonic condition and therefore its $\boldsymbol{C_d}$ is lower while 2,24 mm Venturi nozzle diameter has a higher $\boldsymbol{C_d}$ because the throat flow is almost sonic condition, ***Ma*** was estimated in the throat's center.

Best calibration points for both Venturi nozzles occur under low relation values $1/\boldsymbol{Re}^{0,5}$, which means, regimen flow is about to stop being viscous, and is close to sonic condition, for example, for ***d*** = 2,24 mm its best calibration point is $\boldsymbol{C_d}$ = 0,9696 for a regime ***Re*** = 24338,66 and ***Ma*** = 0,972, see tables 4 and 6. However, for ***d*** = 0,56 mm nozzle every calibration point in the flow are in a total viscous and subsonic regime, so the discharge coefficient has dissipative, dynamics and hydrostatic unwished effects, since the maximum value is $\boldsymbol{C_d}$ = 0,8984 with ***Re*** = 4666,57 and ***Ma*** = 0,899, see tables 3 and 4.

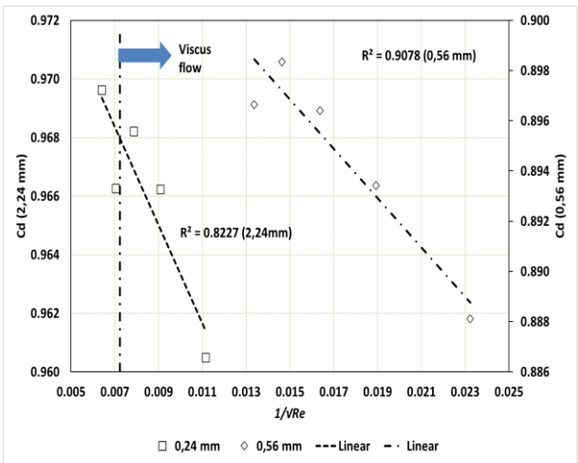

Graphic 2 C_d vs $1 / Re^{0,5}$
Source: Own elaborated

$$C_d = 0{,}9116 - \frac{0{,}9819}{\sqrt{Re}} \tag{22}$$

$$C_d = 0{,}9801 - \frac{1{,}6807}{\sqrt{Re}} \tag{23}$$

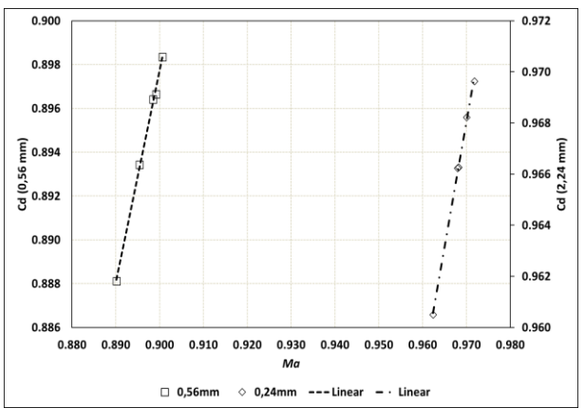

Graphic 3 Compressible Flow in the throat, C_d vs Ma
Source: Own elaborated

From the shown data, it is important to understand the totally viscous compressible flow mechanism about the realized calibration and above all to understand how this flow regimen affects the discharge coefficient magnitude, thus, by using computational fluid dynamics (CFD) an experiment in totally viscous regimen is realized, the software ANSYS® 2020 R1 student's version is used.

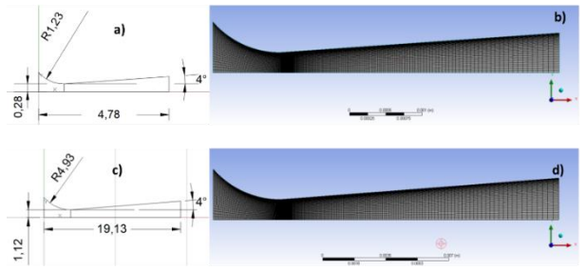

Figure 1 Venturi nozzle geometries and computational space discretization
Source: own elaborated

Figures 1a y 1c, show the principal dimensions for ***d*** = 0,56 mm and ***d*** = 2,24 m Venturi nozzles, respectively. Figures 1b and 1d show discretization of the computational space with structured meshing, where ***d*** = 0,56 mm Venturi has a density of 10459 elements and ***d*** = 2,24 mm has a density of 10234 elements, it also shows the logarithmic increase of the mesh for the wall and the throat zone to obtain a good estimation of the throat velocity profiles. The numerical experimental conditions are: symmetric-axis, stationary, ideal gas (air), turbulence model ***k-ε*** realizable, solver density-base. The experiment got solved for Pressure-inlet-Pressure-outlet conditions, where boundary conditions for the entrance are total pressure P_0 and entrance temperature T_0, showed in tables 3 and 4. According to results discussed on Graph 3, global flow in the throat is ***Ma*** <1, this is the reason why in the Venturi exit plane the only back pressure will be atmospheric pressure, thus, to determinate the exit boundary condition is needed the Venturi nozzles geometries, knowing them, the area between the throat and the exit plane is determined, A_e/A^*, using this result and the interpolation of isentropic relations for an ideal gas (γ = 1.4), Ma_e and P_e/P_0 can be known in the exit plane of the Venturi nozzles, see Table 7.

Diameter	A_e/A^*	P_e/P_0	Ma_e
0,56 mm	1.96	0,098	2,17
2,24mm	2.1	0,087	2,25

Table 7 Isentropic relations in the exit plane
Source: Own elaborated

The obtained results from the numerical experiment are shown in Graph 4. The figure shows the velocity profiles of Blassius ***u/U,*** as a function of ***r/d*** for each diameter throat and each stagnation pressure. The standard velocity profile has a cero value on the wall, so the separation gets the boundary layer thickness ***r*** = ***δ(x),*** the standard velocity profile reaches its maximum value ***u/U*** = 0,99 in supersonic regime ***Ma*** > 1. The flow acceleration in the boundary layer is caused by the viscous dissipation, since the friction between the flow and the wall increases the flow internal energy, and by consequence, the temperature increase will cause a decrease the flow density, the flow must accelerate in the small displacement thickness ***δ****. Outside the viscous zone flow is subsonic, and the relation ***u/U*** will be more sensible to the pressure gradients change ***dP/dr***, see Graph 4 and 5. From Graph 5, outside the boundary layer, gradient is unfavorable, ***dP/dr*** > 0, flow is adverse and the profile ***u/U*** decreases against the flow direction. In the wall region the gradient is favorable, ***dP/dr*** < 0, the profile ***u/U*** increases in the flow direction and reaches its maximum value in viscous zone limit.

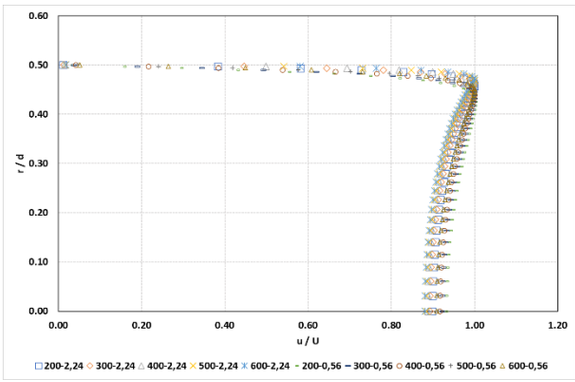

Graphic 4 Standard velocity profiles, 0,56 y 2,24 mm
Source: Own elaborated

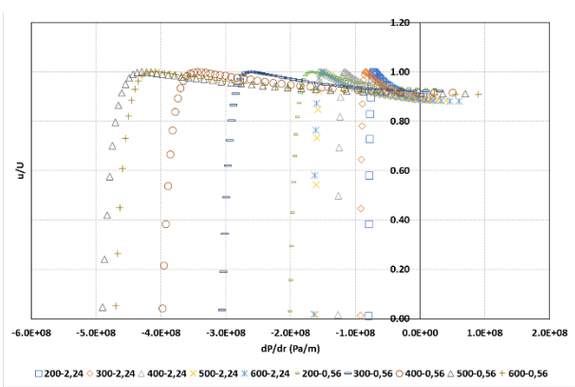

Graphic 5 Profile u/U vs dP/dr, 0,56 y 2,24 mm
Source: Own elaborated

ISSN: 2410-3454

The standard velocity profile is used to find the displacement thickness ***δ*/d*** in the throat, thus, pressure gradient in the wall is considered as zero, ***dP/dx*** = 0 [18; 19] and the velocity profile behavior will be approximate to a laminar and parabolic behavior in the boundary layer thickness. To sustain the laminar and parabolic velocity profile consideration, the shape factor ***H*** was calculated, thus, Jea-Hyung equations are used [11] to calculate the displacement thickness ***δ**** and the moment thickness ***θ,*** the results are shown in Graph 6. In the Figure is appreciated factor ***H*** depends on the throat diameter, the stagnation pressure, and the pressure gradient in the wall zone. Outside the viscous region, ***H*** is independent of ***r/d,*** therefore, ***H*** approximates to a constant and will only be lightly modified by the pressure gradient. The red and blue color ovals in the figure indicate the immediate zone on the wall where viscous effects predominate, as value ***H*** > 2,0 indicates, and particularly in the throat diameter of 0,56 mm this effect is remarkable since despite stagnation pressure increases and by consequence velocity increases as well, the ***H*** difference is 0,24 % in the test interval. In both throat diameters flow is totally laminar on the wall zone, as reported [18], therefore a parabolic and laminar profile approximation can be used in the boundary layer thickness.

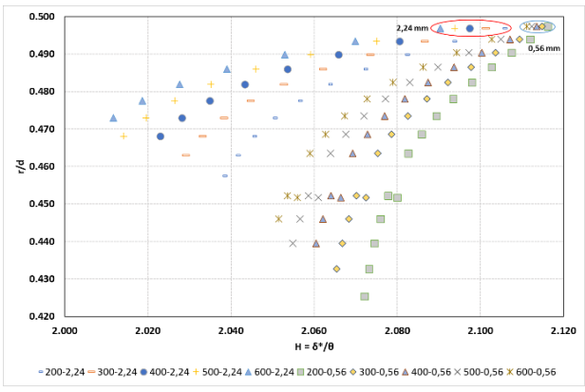

Graphic 6 Shape factor H, 0,56 y 2,24 mm
Source: Own elaborated

The literature stablished [5;20] the boundary layer thickness ***δ*** has its maximum value when ***u/U*** = 0,99, using this consideration, in Graph 4 results, dispersion data from the wall to the maximum value ***δ(x)*** are extracted, see Graphs 7 and 8. The figures show the standard profiles in the boundary layer thickness ***δ*** for the throat diameters, it also shows the data adjust and the adjust quality factor which indicates the good adjust quality, since $R^2 \approx 1$, figure presents too the adjust equations obtained.

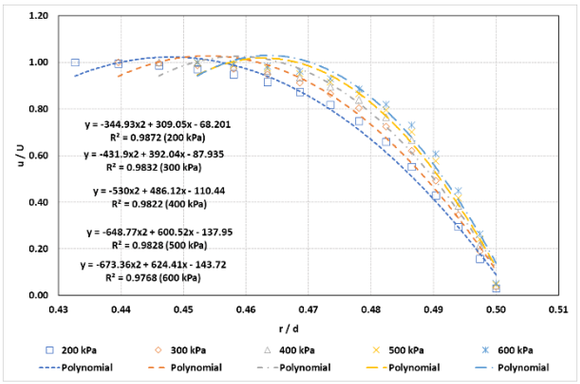

Graphic 7 Standard profiles in viscous zone, 0,56 mm
Source: Own elaborated

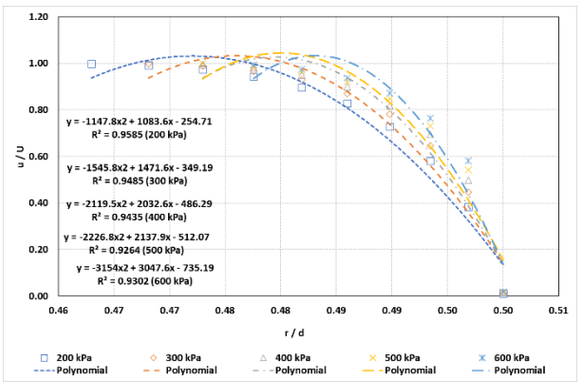

Graphic 8 Standard profiles in viscous zone, 2,24 mm
Source: Own elaborated

Substituting velocity profiles equations in the momentum integral equation for a zero-pressure gradient, the thickness movement ***δ**** in function of ***Re*** and the flat-plate's longitude ***x***. To obtain the equation as function of the throat diameter the Stratford equation [18] for equivalent length must be used. In Graph 9 shows obtained results, the ***δ*/d*** behavior is linear from the region near the wall to the boundary layer thickness, the ovals in the graphic point out the maximum value of the relation ***δ*/d*** which belongs to the thickness movement for each throat diameter and stagnation pressure**.** The viscous regime is superior in the Venturi nozzle of 0,56 mm diameter hence it has the higher values of ***δ*/d,*** and because the flow velocity is higher in the throat diameter of 2,24 mm the viscous effects affect in less proportion the thickness movement, since it has lower values of relation ***δ*/d*** than the other diameter under the same stagnation conditions. From the movement thickness data, the lineal adjust is realized as shown is Graph 9, in the figure is also seen the good quality of the adjust, since $R^2 \approx 1$, the equations 24 is the lineal variation of the relation ***δ*/d*** as function of the flow regime.

ISSN: 2410-3454

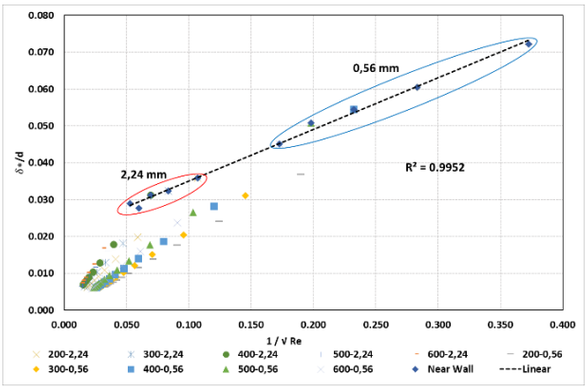

Graphic 9 Movement thickness as function of $Re^{-0,5}$
Source: Own elaborated

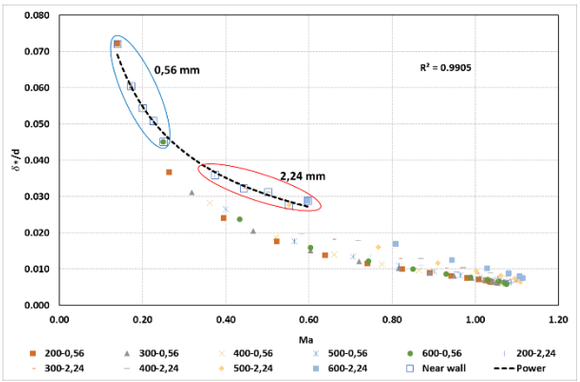

Graphic 10 Thickness movement in function of Ma
Source: Own elaborated

$$\frac{\delta^*}{d} = 0{,}021 + \frac{0{,}1401}{\sqrt{Re}} \tag{24}$$

Earlier was discussed the importance of flow compressibility in the throat nozzle, see Graph 3, in that sense, the ***δ*/d*** relation is shown in Graph 10 as a function of ***Ma*** number. In the graph is shown the variation of the relation ***δ*/d*** as function of ***Ma*** from the movement thickness to the boundary layer thickness. In the thickness of movement (ovals) is appreciated that compressibility reduces the thickness ***δ*/d*** dimension and thence improves the throat strangulation; the 2,24 mm throat has a value of 35,92% smaller than 0,56 mm in equal conditions of stagnation, 600 kPa, which provokes a better estimation of C_d for this throat diameter. Using the data in the thickness of movement an adjust is realized, in the graph is shown the good quality of the adjust, since $R^2 \approx 1$.

$$\frac{\delta^*}{d} = 0{,}0196Ma^{-0{,}64} \tag{25}$$

Equation 25 is the potential variation of the relation ***δ*/d*** as a function of Mach number, this proposition's objective is to estimate the size and behavior of the thickness of movement by the flow compressibility, this equation is proposed to be used for the interval $0{,}14 \leq Ma \leq 0{,}6$, and presents the necessity of realized another studies to validate this empirical model.

Given that viscosity and compressibility effects affection on the thickness of movement size were widely discussed, now is proceeded to the estimation of the discharge coefficient, Stratford [18] reported that the discharge coefficient in the viscous region is $(1 - C_{dvis}) = 4\delta^*/d$, with the thickness of movement results, the C_{dvis} in the viscous is estimated, the equation 26 represents the C_{dvis} variation for throat diameters of 0,56 and 2,24 mm.

$$C_{dvis} = \frac{0{,}5604}{\sqrt{Re}} \tag{26}$$

Now the discharge coefficient in the free stream zone is determined, $C_{d\text{-}inv}$, Cruz Maya [8] developed an integral equation for momentum along the sonic line for stationary, compressible, dimensionless, and uniform properties flow, see equation 27, where ρ is the density, a is the sound's velocity in the throat, γ is the specific heat relation under stagnation conditions and P is the static pressure in the throat.

$$C_{dinv} = \left(\frac{\rho a^2}{\gamma_0 P}\right)_{th} \tag{27}$$

From results of the numerical experiment C_{dinv} is calculated as function of radial position, as Cruz-Maya said the term $(\rho\ a^2/\ P)$ takes different values in the radial plane of the nozzle throat, combining rests between the limits of 0 and 1, and for each stagnation pressure and throat diameter the results are ***0,9945*** and ***0,9261*** for 2,24 y 0,56 mm respectively. The total discharge coefficient is C_d = 1- (Cd_{vis}-1) - (Cd_{inv}-1) [8,18], therefore the coefficients end as following:

$$C_d = 0{,}9882 - \frac{0{,}5604}{\sqrt{Re}} \tag{28}$$

$$C_d = 0{,}9261 - \frac{0{,}5604}{\sqrt{Re}} \tag{29}$$

ISSN: 2410-3454

Equations 28 and 29 are the numerical coefficients in flow close to the throat's strangulation for diameter of 2,24 and 0,56 mm respectively, these two models are now compared to experimental results, empirical equations 22 and 23, as well as ISO 93000 [17] and Ishibashi's [7] equation, see graph 11.

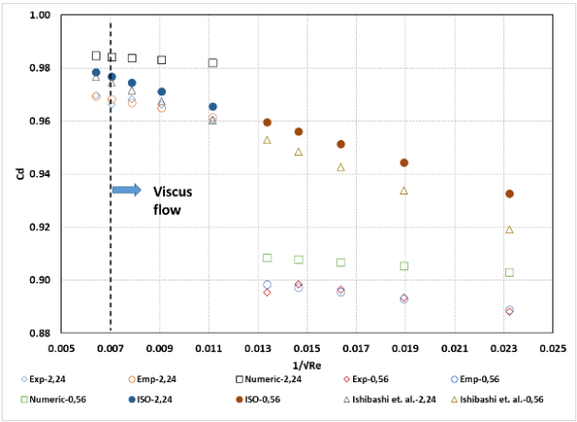

Graphic 11 Numerical, experimental and empirical discharge coefficient for 2,24 and 0,56 mm diameters and comparative
Source: Own elaborated

The discharge coefficients from Figure 12 show in flow regime close to turbulent $1 / Re^{0.5} \approx 0{,}007$ the ISO 9300 and Ishibashi models are close to experimental C_d.

Of 2,24 mm since the maximum error is from 1,07 to 0,84% respectively, however for the numerical model, equation 28, the maximum error is 2,18% for totally viscous zone, the empirical model in equation has a maximum error of 0,2%, it's important to indicate the numerical model's estimation improves as the flow regime approximates to turbulent region, since the minimum error is 1,52%.

With respect to C_d results for 0,56 mm the models of ISO 9300 and Ishibashi have errors of 6,68 and 6,03%, respectively, therefore they're not a good choice for calibration in totally viscous region, in respect of the numerical model it shows an acceptable performance, since the maximum error is 1,64 % and improves the estimation in a way the flow regime increases, finally empirical equation 22, has a maximum error of 0,32 %, meaning it is the best calibration option in totally viscous regime.

Conclusions

Likewise, it can be concluded that:

1. The calibration in $Ma \approx 1$ flow causes dissipative, dynamics and hydrostatic unwished effects on the thickness of movement δ^*, therefore in the C_{dvis} magnitude, and these effects are prevalent for the 0,56 mm throat's diameter since relation δ^* / d is 35,92% bigger than 2,24 mm throat's diameter.

2. Numerical models are a bad estimation of C_d under these stagnation conditions since the maximum error estimated is 6,68% and is superior in the 0,56 mm throat's diameter.

3. The empirical models are a good estimation of C_d since the errors for both Venturi nozzles weren't higher than 1% and for these flow conditions the best option is experimental calibration.

4. 2,24 mm throat diameter can reach better results if the flow regime keeps increasing to get close to sonic condition and therefore avoid static pressure variation affection on the C_d magnitude.

5. The measure uncertainty was satisfactory estimated, therefore good quality on obtained results in this work are assured.

Nomenclature

A	*Surface*
CFV	*Critical Flow Venturi*
c	*Number of pulses*
C^*	*Johnson's critical flow factor*
C_d	*Discharge coefficient of the nozzle*
C_{d-vis}	*Viscous discharge coefficient*
$C_{d-invis}$	*Inviscous discharge coeffient*
d	*Venturi nozzle throat diameter*
δ	*Boundary layer thickness*
δ^*	*Thickness of movement*
K	*National's patron calibration constant*
k	*Coverage factor*
γ	*Specific heats relation*
m_{ideal}	*Ideal mass flow rate*
m_{actual}	*Actual mass flow rate*
Ma	*Mach number*
N	*Contributions number*
Pp	*Pressure patron*
P_0	*Stagnation pressure*
p	*Trust level*
Q	*Volumetric flow rate*
$Rgas$	*Gasses constant*

ISSN: 2410-3454

$\boldsymbol{Re}$ *Reynolds number*
$\boldsymbol{T_P}$ *Patron temperature*
$\boldsymbol{To}$ *Stagnation temperature*
$\boldsymbol{u_{cd}}$ *Discharge coefficient uncertainty*
$\boldsymbol{\rho}$ *Patron's air density*
$\boldsymbol{\mu_0}$ *Viscosity under stagnation conditions*
$\boldsymbol{t}$ *Recollection time of gass*

Superscripts

$\boldsymbol{o}$ *Stagnation conditions*
$\boldsymbol{*}$ *Critical conditions*

Subscripts

e *Output conditions*

Acknowledgement

We thank the Centro Nacional de Metrología (CENAM) for the facilities provided for the calibrations, especially the flow and volume laboratory.

Funding

This work has been funded by the Secretaría de Investigación y Posgrado through project SIP 20221079 of Instituto Politécnico Nacional.

References

[1] A Picard, R. S. (2008). Revised Formula for the Density of Moist Air. *Metrología 45*, 149-155. doi:10.1088/0026-1394/45/2/004

[2] Aaron Johnson, J. W. (2008). Comparison Between Theoretical CFV Flow Models and NIST's Primary Flow Data in the Laminar, Turbulent and Transition Flow Regimes. *Journal of Fluids Engineering ASME*. http://fluidsengineering.asmedigitalcollection.asme.org/pdfaccess.ashx?url=/data/journals/jfega4/27324/ on 07/08/2017

[3] B. Mikan, R. K. (2006). Determination of discharge coefficient of critical nozzles based on their geometry and the theory of laminar and turbulent boundary layers. *Proceedings of the 6th International Symposium on Fluid Flow Measurement*.

[4] Chunhui Lia, P. a. (2018). Throat Diameter Influence on the Flow Characteristics of Critical Venturi Nozzle. *Flow Measurement and Intrumentation* , 105-109. https://doi.org/10.1016/j.flowmeasinst.2018.02.012

[5] Fox, R. W. (2011). *Introduction to Fluid Mechanics.* USA: Wiley and Sons Inc.

[6] (2002). *Guía para la expresión de la incertidumbre en las mediciones.* Norma Mexicana NMX-CH-140-IMNC-2002.

[7] Ishibashi, M. (2015). Discharge Coefficient equation for critical-flow toroidal-throat venturi nozzles covering the boundary-layer transition regime. *Flow Measurement and Instrumentation*, 107-121. http://dx.doi.org/10.1016/j.flowmeasinst.2014.11.009

[8] J. A. Cruz-Maya, F. S. (2006). A new correlation to determine the discharge coefficient of a critical Venturi nozzle with turbulent boundary layer. *Flow Measurement and Instrumentation*, 258-266. doi:10.1016/j.flowmeasinst.2006.06.002

[9] J. M. Lim, B. H.-A. (2011). The humidity effect on air flow rates in a critical flow venturi nozzle. *Flow Measurement and Intrumentation*, 402-405. doi:10.1016/j.flowmeasinst.2011.06.004

[10] J.A., C. M. (2005). Analytical and Numerical Characterization of the Discharge Coefficient of a Sonic Venturi Nozzle. *Ph. D. Thesis Instituto Politécnico Nacional*.

[11] Jae Hyung Kim, H. D. (2010). The Effect of Diffuser Angle on the Discharge Coefficient of a Miniature Critical Nozzle. *Journal of Thermal Science*, 222-227. DOI: 10.1007/s11630-010-0222-2

[12] John D. Wright, W. K. (2021). Thermal boundary layers in critical flow Ventures . *Flow Measurement and Instrumentation*, 102525. https://doi.org/10.1016/j.flowmeasinst.2021.102025

[13] Junji Nagao, S. M. (2013). Characterictics of high Reynolds number flow in a critical nozzle. *International Journal of Hydrogen Energy*, 1-9. http://dx.doi.org/10.1016/j.ijhydene.2013.04.158

[14] Lambert Marc Antoine, R. M. (2021). Experimental Investigations on Cylindrical Critical Flow Venturi Nozzles with Roughness. *Flow Measurement and Instrumentation*, 102002. https://doi.org/10.1016/j.flowmeasinst.2021.102002

[15] Masahiro Ishibashi, M. T. (2000). Theoretical discharge coefficient of a critical circular-arc nozzle with laminar boundary layer and its verification by measurements using super-accurate nozzles. *Flow Measurement and Intruments* , 305-313.

[16] Rivera, J. E. (2006). *Diseño, construcción y caracterización de un banco de toberas sónicas para un laboratorio secundario de medición de flujo de gases.* Mexico.

[17] (1990). *Standard ISO 9300 Critical Measurement of Gass flow by Means of Flow Venturi Nozzles* .

[18] Stratford, B. S. (n.d.). The calculation of the discharge coefficient of profiled choked nozzles and the optimum profile for absolute air flow measurement . *Formely National Gas Turbine Establishment, Pystoch, now Rolls-Royce Ltd.* https://doi.org/10.1017/S0001924000060905

[19] White, F. (2009). *Fluid Mechanics* . USA: McGraw-Hill.

[20] Wolfgan A. Schmid, R. J. (2004). *Guía para la estimación de la incertidumbre* . CENAM.

[21] Wright, J. (1998). The Long Term Calibration Stability of Critical Flow Nozzles and Laminar Flowmeters . *Proceedings of the 1998 NCSL Workshop and Symposium (Standard ISO 9300 Critical Measurement of Glass flow by Means of Flow Venturi Nozzles, 1990)*, 443-462.

ISSN: 2410-3454

Article **Journal of Engineering Applications**

June 2023, Vol.10 No.29 13-20

Development of prototype and measurement, control and automation system in real time for small production greenhouses

Desarrollo de prototipo y sistema de medición, control y automatización en tiempo real para invernaderos de pequeña producción

MUÑOZ-FLORES, Cristofer Alexis†, SOTO-MORALES, Emilia Itzel†, HERRERA-DIAZ, Israel Enrique* and GAMIÑO-RAMIREZ, Edith Alejandra

Universidad de Guanajuato, CIS, División de Ciencias de la Vida, DIA, México.
Universidad de Guanajuato, CCS, División de Ciencias de la Salud e Ingenierías, DEC, México.

ID 1st Author: *Cristofer Alexis, Muñoz-Flores*

ID 1st Co-author: *Emilia Itzel, Soto-Morales*

ID 2nd Co-author: *Israel Enrique, Herrera-Diaz* / **ORCID:** 0000-0002-2117-7548, **CVU CONAHCYT ID:** 207880

ID 3td Co-author: *Edith Alejandra, Gamiño-Ramirez*

DOI: 10.35429/JEA.2023.28.10.13.20 Received: January 15, 2023; Accepted: June 30, 2023

Abstract

The main objective of this work is to develop a real-time control system and accessible instrumentation for small production greenhouses located in the State of Guanajuato; whose goal is to increase production, make optimal use of the irrigation system and efficient water management. For this, a prototype of a greenhouse irrigation system was built with the inclusion of temperature sensors, environmental relative humidity, flowmeters, solenoid solenoid valves and soil humidity sensors, these values are compared with a numerical model to corroborate the magnitudes obtained and assess the delivery of flow and irrigation time in each section of the laboratory greenhouse. The development of a graphical interface in LabVIEW for the control and operation of sensors and the complete irrigation system stands out, being this quite intuitive and easy to use for a farmer. The results obtained from the work show differences between the measured and modeled of the hydrodynamic variables in a range of 8 to 10%, where it is concluded in an improvement in the development of the code in Arduino for its optimization in response time and migration to mobile platforms.

Greenhouse, Control, Measurement

Resumen

El presente trabajo tuvo como objetivo principal el desarrollar un sistema de control en tiempo real e instrumentación accesible para invernaderos de pequeña producción ubicados en el Estado de Guanajuato; cuya meta es aumentar la producción, hacer un uso óptimo del sistema de riego y manejo eficiente del agua. Para ello se construyó un prototipo de sistema de riego de invernadero con la inclusión de sensores de temperatura, humedad relativa ambiental, caudalímetros, electroválvulas solenoide y sensores de humedad de suelo, estos valores son comparados con un modelo numérico para corroborar las magnitudes obtenidas y valorar la entrega de caudal y tiempo de riego en cada sección del invernadero del laboratorio. Se destaca el desarrollo de una interfaz gráfica en LabVIEW para el control y operación de sensores y del sistema completo de riego, siendo este bastante intuitivo y de fácil manejo para un agricultor. Los resultados obtenidos del trabajo arrojan diferencias entre lo medido y modelado de las variables hidrodinámicas en un rango del 20 al 30%, donde se concluye en una mejora en el desarrollo del código en Arduino para su optimización en tiempo de respuesta y migración a plataformas móviles.

Invernadero, Medición, Control

Citation: MUÑOZ-FLORES, Cristofer Alexis, SOTO-MORALES, Emilia Itzel, HERRERA-DIAZ, Israel Enrique and GAMIÑO-RAMIREZ, Edith Alejandra. Development of prototype and measurement, control and automation system in real time for small production greenhouses. Journal of Engineering Applications. 2023. 10-29:13-20.

* Correspondence of the Author (E-mail: eherrera@ugto.mx)
† Researcher contributing as first author.

Introduction

Smart greenhouses are structures designed to provide a controlled environment for growing plants (Diaz et. al., 2019). These greenhouses use advanced technology to monitor and control factors such as temperature, humidity, light, and air composition.

These greenhouses are often equipped with sensors and automation systems that allow growers to monitor and control the growing environment remotely (Xia et. al., 2020). For example, sensors can measure temperature and humidity in real time and automatically adjust heating, ventilation, and irrigation systems to maintain an optimal environment for plant growth (Garcia et. al., 2020).

The main difference between a traditional greenhouse and a smart greenhouse lies in the degree of automation and control that can be achieved through the use of advanced technology (Wang et. al., 2018).

In a traditional greenhouse, growers rely mainly on their experience and knowledge to regulate environmental conditions, such as temperature, humidity, and lighting. This may involve manual adjustments in opening and closing windows, manual watering of plants, and constant monitoring of conditions inside the greenhouse (Li, et. al., 2018) (Li et. al., 2020).

On the other hand, a smart greenhouse incorporates technology to automate and optimize these processes. Sensors continuously monitor environmental conditions, collecting accurate data on temperature, humidity, soil quality, among others. This data is used by automated control systems to adjust and maintain the ideal parameters for plant growth.

Some of the specific differences between a traditional greenhouse and a smart greenhouse are (Liu et. al., 2019):

1. Precise control of conditions: In a traditional greenhouse, farmers must make manual adjustments based on their experience and observation. In contrast, a smart greenhouse uses sensors and automated systems to monitor and adjust environmental conditions precisely and constantly.

2. Resource optimization: Smart greenhouses are designed to maximize efficiency in the use of resources such as water, energy and nutrients. Irrigation and fertilization systems can be adjusted according to the specific needs of the plants, avoiding waste and optimizing growth.

3. Programming and automation: Smart greenhouses can be programmed to mimic natural light and temperature cycles, simulate seasons, and adapt to different stages of plant growth. In addition, many tasks can be automated, such as regulating lighting, ventilation and irrigation, reducing the manual intervention required.

4. Remote monitoring and control: Smart greenhouses allow growers to monitor and control greenhouse conditions remotely. This means they can receive notifications on their mobile devices about any changes in conditions, as well as adjust parameters from anywhere with an Internet connection.

Therefore, a smart greenhouse uses advanced technology, sensors and automated systems to provide precise and optimized control of plant growth conditions (Li et. al., 2020). This allows for greater efficiency, more rational use of resources and optimization of agricultural processes, compared to a traditional greenhouse that relies heavily on the experience and manual intervention of the farmer (Martinez, et. al., 2019) (Rallo et. al., 2019).

The present research work presents measurement and control development to optimize not only water distribution lines for irrigation by seeking to make water use more effective, but also the monitoring of environmental variables (air humidity, temperature, etc.) as well as a monitoring of greenhouse conditions for decision making.

It is worth mentioning that the development of low-cost control and monitoring allows small greenhouse growers of both crops and ornamental plants to have within reach a system that helps them to control irrigation times.

ISSN: 2410-3454

MUÑOZ-FLORES, Cristofer Alexis, SOTO-MORALES, Emilia Itzel, HERRERA-DIAZ, Israel Enrique and GAMIÑO-RAMIREZ, Edith Alejandra. Development of prototype and measurement, control and automation system in real time for small production greenhouses. Journal of Engineering Applications. 2023

On the other hand, the development of this control and instrumentation proposal will allow future projects and research to have a reliable basis that they can analyze, increasing their range of options and deciding whether it is useful or not without having to conduct research on their own to find out. Finally, once the general objective of this research has been achieved, it will be a beneficial contribution not only for the economic and hydraulic sector, but it will also mean an advance for those producers who need to control and monitor their productions.

Materials and Methods

Governing equations

For the analysis of pressure flow in pipes, the energy equations are used, associated with the continuity equation and the friction and fitting loss formulations (Figure 1). The variables involved in simple pipe problems are as follows:

Variables related to the pipe itself: pipe diameter (d), pipe length (l) and absolute pipe roughness (ks).

Variables related to the fluid: fluid density (ρ) and fluid dynamic viscosity (μ).

Variables related to the system layout: Minor loss coefficients (hm) in all necessary fittings, including valves, as well as friction losses (hf) (Potter et al., 2002).

Variables related to fluid driving energy: Head between inlet and outlet reservoir (H) or pump power (P).

Other variables: Gravity acceleration (g) and flow rate or average velocity in the pipe (Q or v). By using the Bernoulli (eq. 1), Colebrook-White (eq. 2) equations together with the Darcy-Weisbach equation (eq. 3) we have:

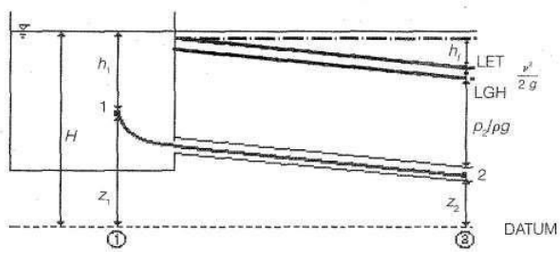

Figure 1 Representative diagram of a pipe. Point 1 is located well inside the tank in such a way that its velocity is approximately O. Point 2 is located downstream in the flow within the pipe
Source: (Saldarriaga, 1998)

$$\frac{P_1}{\gamma}+\frac{V_1^2}{2g}+z_1=H_p+\frac{P_2}{\gamma}+\frac{V_2^2}{2g}+z_2+H_f \quad (1)$$

$$\frac{1}{\sqrt{f}}=-2log_{10}\left(\frac{e}{3.7D}+\frac{2.51}{Re\sqrt{f}}\right) \quad (2)$$

$$H_f=f\frac{L}{D}\frac{V^2}{2g} \quad (3)$$

An equation (4) in terms of velocity that combines equations (1 to 3) and can be applicable for irrigation piping systems in greenhouses:

$$V=\frac{-2\sqrt{2gDH_f}}{\sqrt{L}}log_{10}\left(\frac{e}{3.7D}+\frac{2.51\nu\sqrt{L}}{D\sqrt{2gDH_f}}\right) \quad (4)$$

This last equation is the basis for the solution of the simple pipe system that forms the greenhouse.

Greenhouse Physical Model

The construction of the piping system for irrigation in a greenhouse was a prototype in the applied mechanics laboratory of the Life Sciences Division of the Irapuato-Salamanca Campus; in it, six downspouts were placed to micro-sprinkler irrigation supply tables as shown in figure (2).

Figure 2 Irrigation system based on six drops with a aspersion

ISSN: 2410-3454

Each downspout has a DC-12V solenoid valve, a flow meter and a soil moisture sensor HL69, this distribution is shown in figure (3).

Figure 3 Detail of installation of lowering in irrigation table

Likewise, there are DHT sensors in each corner of the circulation system that allow obtaining the parameters of temperature and humidity, as shown in figure (4).

Figure 4 Location of the DHT sensor in a corner of the irrigation system

The physical model is fed by a 90 liter tank and a 0.5 HP pump, as well as ball valves for pipe sectioning.

At one end of the installation, there are cable drops for the control of the installation, in figure (5), the connection of the system to a computer is shown.

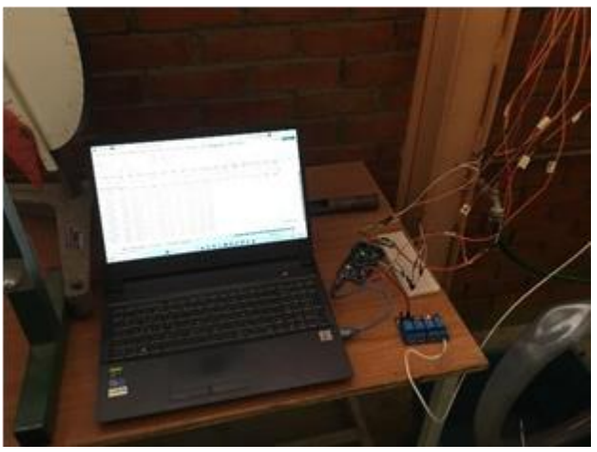

Figure 5 Connection of wires to Arduino and monitoring of values and control of sensors

The physical model of irrigation system installations is numerically modeled to obtain previously the design and characteristics of diameters, pressures, flows and velocities in all pipes.

Numerical Model

The numerical model used to calculate the hydrodynamic variables of the fluid in the pipe was the PIPE FLOW Expert, the software determines the flow, velocities and pressures at the nodes or points of interest. Figure (6) shows the design of the greenhouse piping system.

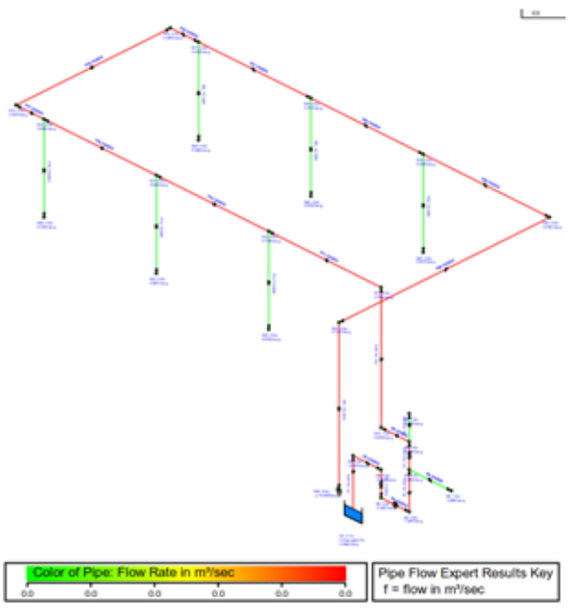

Figure 6 Greenhouse piping system and flow results in the system

ISSN: 2410-3454

The initial values are shown in figure (7).

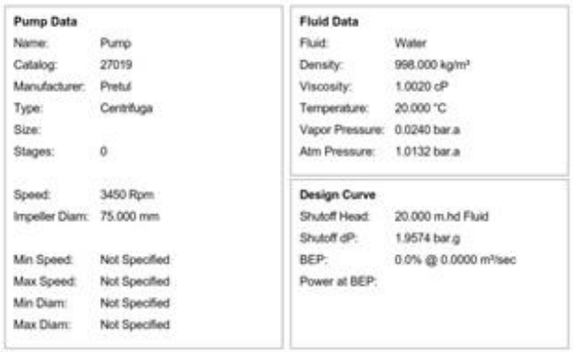

Figure 7 Pump and fluid data in Pipe Flow Expert

Likewise, table (1) shows the pipes used that are PVC Hydraulic Sch. 40, with diameters of 1 inch (25 mm) and 0.5 inch (15 mm), where at the end the values of the flow, velocity and inlet and outlet pressures in each pipe are observed respectively.

Pipe Id	Pipe Name	Material	Inner Diameter	Mass Flow	Flow	/elocit y	Entry Pressure	Exit Pressure
	and Notes		mm	kg/sec	/se c	m/sec	bar.g	bar.g
1	P1	PVC (ANSI) Ced. 40	26.645	1.414	0.001	2.540	0.069	-0.058
2	P2	PVC (ANSI) Ced. 40	26.645	1.414	0.001	2.540	-0.058	-0.087
3	P3	PVC (ANSI) Ced. 40	26.645	1.414	0.001	2.540	-0.087	-0.350
4	P4	PVC (ANSI) Ced. 40	26.645	1.414	0.001	2.540	-0.350	1.325
5	P5	PVC (ANSI) Ced. 40	26.645	1.414	0.001	2.540	1.325	1.286
6	P6	PVC (ANSI) Ced. 40	26.645	0.000	0.000	0.000	1.286	1.286
7	P7	PVC (ANSI) Ced. 40	26.645	1.414	0.001	2.540	1.286	0.998
8	P8	PVC (ANSI) Ced. 40	26.645	0.000	0.000	0.000	0.998	0.980
9	P9	PVC (ANSI) Ced. 40	26.645	1.414	0.001	2.540	0.998	0.971
10	P10	PVC (ANSI) Ced. 40	26.645	1.414	0.001	2.540	0.971	0.783
11	P11	PVC (ANSI) Ced. 40	26.645	1.414	0.001	2.540	0.783	0.719
12	P12	PVC (ANSI) Ced. 40	15.799	0.000	0.000	0.000	0.719	0.875
13	P13	PVC (ANSI) Ced. 40	26.645	1.414	0.001	2.540	0.719	0.654
14	P14	PVC (ANSI) Ced. 40	15.799	0.000	0.000	0.000	0.654	0.809
15	P15	PVC (ANSI) Ced. 40	26.645	1.414	0.001	2.540	0.654	0.590
16	P16	PVC (ANSI) Ced. 40	15.799	0.000	0.000	0.000	0.590	0.744
17	P17	PVC (ANSI) Ced. 40	26.645	1.414	0.001	2.540	0.590	0.558
18	P18	PVC (ANSI) Ced. 40	26.645	1.414	0.001	2.540	0.558	0.461
19	P19	PVC (ANSI) Ced. 40	26.645	1.414	0.001	2.540	0.461	0.436
20	P20	PVC (ANSI) Ced. 40	15.799	0.000	0.000	0.000	0.436	0.589
21	P21	PVC (ANSI) Ced. 40	26.645	1.414	0.001	2.540	0.436	0.371
22	P22	PVC (ANSI) Ced. 40	15.799	0.000	0.000	0.000	0.371	0.523
23	P23	PVC (ANSI) Ced. 40	26.645	1.414	0.001	2.540	0.371	0.307
24	P24	PVC (ANSI) Ced. 40	15.799	0.000	0.000	0.000	0.307	0.458
25	P25	PVC (ANSI) Ced. 40	26.645	1.414	0.001	2.540	0.307	0.235
26	P26	PVC (ANSI) Ced. 40	26.645	1.414	0.001	2.540	0.235	0.138
27	P27	PVC (ANSI) Ced. 40	26.645	1.414	0.001	2.540	0.138	0.000

Table 1 Pipe data in Pipe Flow Expert and results

The results of the numerical model were compared with those measured in the physical model by means of the flow meter sensors.

Results and application

As a result of the operation, control and instrumentation of the greenhouse, a graphic interface was designed in LabVIEW, which allows the integration of the Arduino code and the virtual control of the greenhouse sensors that activate the operation and start-up of the low irrigation system. the following initial conditions:

Variable	Start value	Stop value	peration value
Temperature	24 °C	18 °C	20 °C
Relative humidity	70 %	80 %	75 %
Ground humidity	35 %	55 %	42 %

Table 2 Initial condition and operation conditions values in greenhouse

In the user interface GUI (figure 8), the condition of the system shutdown before starting operations is displayed.

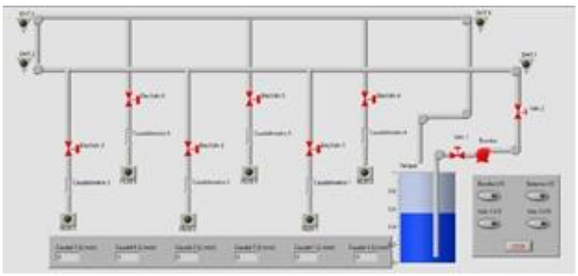

Figure 8 LabVIEW- GUI greenhouse control

Subsequently, the system is turned on (figure 9), obtaining initial values of temperature, relative humidity of the environment and soil humidity to compare with the values that start the irrigation system by opening the solenoid valves and measuring the flow supplied to each section or table depending on the crop and soil moisture conditions.

Figure 9 Start of operation of the greenhouse system

ISSN: 2410-3454

This soil moisture, by indicating a value below the minimum operating value, allows the opening of the solenoid valve to be activated to irrigate the section and quantify the flow that is supplied, as well as the dew time (figure 10); once the maximum system shutdown value for soil moisture has been reached, the solenoid valve closes, ending the water supply in that section according to crop needs.

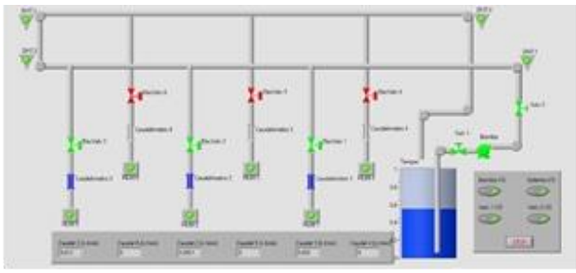

Figure 10 Start of irrigation system in sections 1 and 4

The values of the flows and velocities in pipes for sections 1 to 3 are shown in table (3)

Time	FlowRate (1)	Velocity (1)	FlowRate (2)	Velocity (2)	FlowRate (3)	Velocity (3)
	(L/min)	(m/s)	(L/min)	(m/s)	(L/min)	(m/s)
07:00:00 a. m.	0.13	0.02	0.13	0.02	2.53	0.33
07:00:10 a. m.	0.80	0.11	0.67	0.09	2.00	0.26
07:00:21 a. m.	0.80	0.11	0.27	0.04	2.93	0.39
07:00:31 a. m.	0.53	0.07	0.40	0.05	2.80	0.37
07:00:42 a. m.	0.93	0.12	1.07	0.14	6.53	0.86
07:00:52 a. m.	0.27	0.04	0.40	0.05	3.33	0.44
07:01:03 a. m.	0.40	0.05	0.27	0.04	2.80	0.37
07:01:24 a. m.	0.93	0.12	0.67	0.09	7.87	1.04
07:01:34 a. m.	0.67	0.09	0.13	0.02	3.47	0.46
07:01:45 a. m.	0.40	0.05	0.27	0.04	5.73	0.75
07:01:55 a. m.	0.40	0.05	0.40	0.05	6.13	0.81
07:02:06 a. m.	1.20	0.16	1.07	0.14	8.13	1.07
07:02:27 a. m.	0.40	0.05	0.40	0.05	3.20	0.42
07:02:37 a. m.	0.67	0.09	1.07	0.14	3.20	0.42
07:02:47 a. m.	0.13	0.02	0.40	0.05	2.93	0.39
07:02:58 a. m.	2.00	0.26	1.20	0.16	8.80	1.16
07:03:08 a. m.	1.07	0.14	1.20	0.16	8.53	1.12
07:03:19 a. m.	0.27	0.04	0.13	0.02	2.40	0.32
07:03:50 a. m.	0.27	0.04	0.67	0.09	3.20	0.42
07:04:01 a. m.	0.80	0.11	0.67	0.09	4.13	0.54
07:04:11 a. m.	4.67	0.61	3.73	0.49	26.93	3.54
07:04:32 a. m.	0.00	0.00	0.13	0.02	0.27	0.04
07:04:43 a. m.	0.80	0.11	0.80	0.11	5.47	0.72
07:05:14 a. m.	4.40	0.58	4.13	0.54	24.53	3.23
07:05:24 a. m.	2.67	0.35	2.00	0.26	10.93	1.44
07:05:35 a. m.	3.60	0.47	2.93	0.39	33.73	4.44
07:05:45 a. m.	1.07	0.14	0.93	0.12	6.80	0.89
07:06:06 a. m.	0.67	0.09	0.67	0.09	3.47	0.46
07:06:38 a. m.	0.53	0.07	0.53	0.07	3.33	0.44
07:06:48 a. m.	1.87	0.25	1.60	0.21	15.20	2.00
07:07:09 a. m.	0.53	0.07	0.40	0.05	6.00	0.79
07:07:30 a. m.	1.20	0.16	1.07	0.14	7.60	1.00
07:07:40 a. m.	1.07	0.14	0.67	0.09	12.53	1.65
07:08:01 a. m.	0.53	0.07	0.40	0.05	2.67	0.35
07:08:12 a. m.	2.27	0.30	1.47	0.19	14.00	1.84
07:08:22 a. m.	4.00	0.53	3.47	0.46	28.67	3.77
07:08:43 a. m.	11.87	1.56	11.33	1.49	63.87	8.40
07:08:54 a. m.	5.20	0.68	4.27	0.56	34.27	4.51
07:09:04 a. m.	0.80	0.11	0.67	0.09	8.00	1.05
07:09:25 a. m.	5.20	0.68	5.47	0.72	37.20	4.89
07:09:36 a. m.	0.40	0.05	0.27	0.04	2.40	0.32
07:09:46 a. m.	0.93	0.12	0.80	0.11	4.53	0.60
07:09:57 a. m.	4.00	0.53	2.53	0.33	17.33	2.28
07:10:28 a. m.	3.20	0.42	2.13	0.28	12.67	1.67
07:10:38 a. m.	2.00	0.26	1.73	0.23	10.80	1.42
07:10:49 a. m.	1.07	0.14	1.07	0.14	10.40	1.37
07:10:59 a. m.	2.93	0.39	2.80	0.37	15.07	1.98
07:11:10 a. m.	3.47	0.46	3.87	0.51	25.07	3.30
07:11:20 a. m.	2.00	0.26	1.47	0.19	12.80	1.68
07:11:31 a. m.	2.00	0.26	1.33	0.18	15.60	2.05
07:11:41 a. m.	0.93	0.12	0.93	0.12	6.13	0.81
07:11:52 a. m.	1.73	0.23	1.33	0.18	10.67	1.40
07:12:02 a. m.	0.80	0.11	0.67	0.09	6.13	0.81
07:12:13 a. m.	0.80	0.11	0.67	0.09	7.60	1.00
07:12:33 a. m.	0.13	0.02	0.40	0.05	3.73	0.49
07:12:44 a. m.	0.93	0.12	0.53	0.07	9.20	1.21
07:12:54 a. m.	1.20	0.16	1.33	0.18	14.80	1.95
07:13:05 a. m.	0.40	0.05	0.40	0.05	6.80	0.89
07:13:15 a. m.	6.40	0.84	5.20	0.68	56.53	7.44
07:13:26 a. m.	2.80	0.37	2.13	0.28	19.20	2.53
07:13:36 a. m.	0.93	0.12	1.07	0.14	6.53	0.86
07:13:47 a. m.	4.00	0.53	1.73	0.23	10.53	1.39
07:13:57 a. m.	2.93	0.39	2.27	0.30	22.53	2.96
07:14:08 a. m.	1.73	0.23	0.40	0.05	3.07	0.40
07:14:18 a. m.	2.40	0.32	0.27	0.04	8.80	1.16
07:14:29 a. m.	2.67	0.35	0.67	0.09	10.27	1.35
07:15:00 a. m.	1.47	0.19	1.47	0.19	14.27	1.88

Table 3 Flow values supplied to sections 1 to 3

It is worth mentioning that the response time is reduced by approximately 100 ms, adjustments are currently being made to reduce the response time of the system and make the code optimal (figure 11).

ISSN: 2410-3454

Figure 11 Arduino code section in green-house system

The speed and flow values obtained from the measurement are plotted with respect to time and depending on the needs of each crop, for this case, two irrigation needs of 0.0014 L/min (flow meters 1 and 2) and a third are used. of 0.015 L/min (flow meter 3), obtaining as shown in the graph (1).

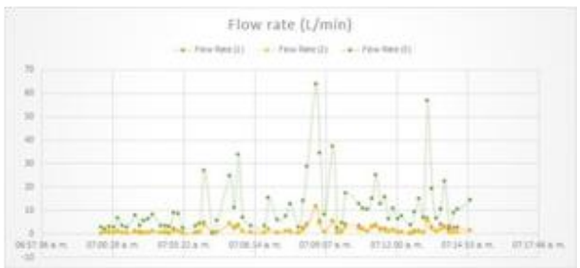

Graphic 1 Flow rate in flow meter 1 to 3

Applying the continuity equation in pipes, the velocity of flow in the pipe is obtained as shown in graph (2).

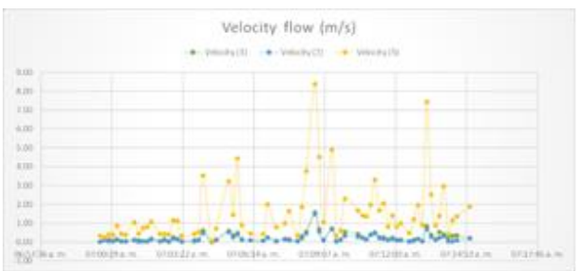

Graphic 2 Velocity flow in flow meter 1 to 3

Conclusions

The development and construction of the instrumentation and control prototype has made it possible to obtain, operate and control different irrigation zones (downspouts or pipes) that have different irrigation needs, taking into account environmental parameters such as relative humidity and temperature, as well as the use of minimum values of soil or substrate moisture, the need to provide a certain flow rate for a determined irrigation time.

The comparison of the flow results obtained by the numerical modeling and those measured by the flowmeter system has a difference between 20% and 33% in magnitude, where it is estimated that this difference is caused by the efficiency curve of the pump and possible differences in construction conditions; however, the operation results with the use of the LabVIEW interface allow to have control of the system in its entirety and provide a necessary flow to each section depending on the requirements of the crop, such as irrigation sheet, irrigation time and control substrate moisture.

The relevance of the design and construction of this prototype allows to have a low installation cost in instrumentation and control, where the development of the graphic interface and the Arduino code can be provided to the farmer for its use, or with the necessary adjustments in number scaling of sensors to satisfy the needs of each crop inside a greenhouse.

References

1. Díaz-Pérez, M., & Gómez-Montoya, D. (2019). A review of IoT-based monitoring and control systems for smart greenhouses. Computers and Electronics in Agriculture, 165, 104955.

2. García-Medina, S., Álvarez, S., Alesanco, Á., & Montero, F. (2020). An IoT Architecture for Intelligent Greenhouses with Context-Aware Decision Support. Sensors, 20(19), 5479.

3. Li, J., Jin, X., Zhu, G., & Chen, Y. (2018). An IoT-based intelligent control architecture for greenhouse environment. Future Generation Computer Systems, 81, 430-441.

4. Li, X., Jia, Z., & Jiang, S. (2020). Research on greenhouse environmental control system based on internet of things. In 2020 5th International Conference on Energy, Environment and Sustainable Development (ICEESD) (pp. 335-339). IEEE.

ISSN: 2410-3454

5. Liu, X., Huang, H., & Chen, G. (2019). Intelligent greenhouse control system based on wireless sensor network and Internet of Things. Journal of Physics: Conference Series, 1396(3), 032063.

6. Li, Y., Cao, Q., & Zhang, Q. (2020). Greenhouse environment monitoring and control system based on the internet of things. In 2020 IEEE 4th Information Technology, Networking, Electronic and Automation Control Conference (ITNEC) (pp. 911-915). IEEE.

7. Martínez, R., & Molina, A. (2019). IoT Architecture for Greenhouse Environment Monitoring and Control. Sensors, 19(13), 2984.

8. Potter, M. C. (2002). Mecánica de Fluidos (3a. ed.). México: Thomson.

9. Rallo, P., & Camacho, E. (2019). Smart Greenhouse Agriculture: A Comprehensive Review. Journal of Clean Energy Technologies, 7(5), 387-391.

10. Saldarriaga V., J. G. (2004). Hidráulica de Tuberías (1a. Ed., 1a. Reimp.). Bogota: Mcgraw-Hill Interamericana.

11. Wang, Z., Wu, J., & Jia, H. (2018). Design and implementation of intelligent control system for greenhouse environment based on internet of things. In 2018 4th International Conference on Control, Automation and Robotics (ICCAR) (pp. 512-516). IEEE.

12. Xiao, H., Li, J., & Zhang, Y. (2020). A smart greenhouse control system based on the internet of things and wireless sensor networks. IEEE Access, 8, 42042-42051.

ISSN: 2410-3454

Article **Journal of Engineering Applications**
June 2023 Vol.10 No.29 21-27

Improvement of the efficiency in the injection process in a company of the automotive sector through the implementation of the SMED (Single-Minute Exchange of Die) methodology

Mejora de la eficiencia en el proceso de inyección en una empresa del sector automotriz mediante la implementación de la metodología SMED (Single-Minute Exchange of Die)

VÁZQUEZ-ROSAS Sergio†*, HERNÁNDEZ-SÁNCHEZ Uriel Alejandro, CABALLERO-LÓPEZ Emma Isabel and VALLEJO-HERNANDEZ Arely.

Ingeniería en Mantenimiento Industrial, Universidad Tecnológica del Centro de Veracruz, Av. Universidad 350, Cuitláhuac, C.P. 94910, Veracruz, México

ID 1st Author: *Sergio, Vázquez-Rosas* / **ORC ID**: 0000-0002-3259-382X, Researcher ID Thomson: P-8011-2018, **CVU CONACYT ID**: 857794

ID 1st Co-author: *Uriel Alejandro, Hernandez-Sánchez* / **ORC ID**: 0000-0003-1488-3601, **Researcher ID Thomson**: Q-2907-2018, **CVU CONACYT ID**: 482289

ID 2nd Co-author: *Emma Isabel, Caballero-López* / **ORC ID**: 0000-0002-6486-9368, **Researcher ID Thomson**: ABH-3859-2020, **CVU CONACYT ID**: 660625

ID 3rd Co-author: *Arely, Vallejo-Hernández* / **ORC ID**: 0000-0001-9249-5458, **Researcher ID Thomson**: O-3653-2018, **CVU CONACYT ID**: 664144

DOI: 10.35429/JEA.2023.29.10.21.27 Received: January 30, 2023; Accepted: June 30, 2023

Abstract

This work was carried out in order to reduce the excessive time in the changes of injection molds, both for aluminum and wood, each of these in their respective pilot areas that were implemented within strategic points were of great help to detect other areas of opportunity for injection in general. However, the equipment and molds used in the injection process are expensive, therefore, the use for product customization in the automotive industry forces the companies that supply inputs to the assemblers to reduce defects and downtime. The results obtained with the implementation of the present methodology generated positive numbers with respect to the time for mold change, obtaining a record change time of 15 minutes, demonstrating that if we look for the appropriate conditions and the necessary tool, we can have the minimum time in addition to obtaining also a maximum time of 3 hours and obtaining a saving of over 93 % equivalent to 255,549.37 USD.

SMED, Automotive industry, Efficiency, Process improvement, Loss reduction

Resumen

El presente trabajo se realizó para poder reducir el excesivo tiempo en los cambios de moldes de inyección tanto de aluminio como de madera, cada uno de estos en sus respectivas áreas piloto que se implementaron dentro de puntos estratégicos fueron de gran ayuda para detectar otras áreas de oportunidad para inyección en general. Sin embargo, los equipos y moldes utilizados en el proceso de inyección son costosos, por consiguiente, el uso para la personalización de productos en la industria automotriz obliga a las empresas que proveen de insumos a las ensambladoras exigen la disminución de defectos y tiempos muertos. Los resultados obtenidos con la implementación de la presente metodología generaron números positivos con respecto al tiempo por cambio de molde obteniendo un tiempo récord de cambio de 15 minutos, demostrando que si buscamos las condiciones apropiadas y la herramienta necesaria podremos tener el mínimo de tiempo además de obtener también un tiempo máximo de 3 horas y obteniendo un ahorro por encima del 93 % equivalentes a 255,549.37 USD.

SMED, Industria automotriz, Eficiencia, Mejora de proceso, Reducción de pérdidas

Citation: VÁZQUEZ-ROSAS Sergio, HERNÁNDEZ-SÁNCHEZ Uriel Alejandro, CABALLERO-LÓPEZ Emma Isabel and VALLEJO-HERNANDEZ Arely. Improvement of the efficiency in the injection process in a company of the automotive sector through the implementation of the SMED (Single-Minute Exchange of Die) methodology. Journal of Engineering Applications. 2023. 10-29: 21-27

*Correspondence to Author (e-mail: sergio.vazquez@utcv.edu.mx)
† Researcher contributing as first author.

Introduction

Products that are used on a daily basis are mostly made by injection moulding, the most common materials that go through this process are; plastics and metals. Regardless of the material, this type of production is complex due to the amount of parts that are used in the moulding of the materials (Pacheco & Heidrich, 2023). To achieve the injection moulding process a certain amount of time is required to generate the quality parameters after performing a mould change (Kemal Karasu et al., 2014). An assembly can be defined as the set of activities in which equipment is prepared or configured for product manufacturing (da Silva & Godinho Filho, 2019). The methodology that has so far proven to support the reduction of downtime is Single Minute Exchange of Die (SMED). To achieve greater efficiency in the processes of changing, adjusting or testing tooling, SMED has been developed as a technique that supports the implementation of lean manufacturing (Lozano et al., 2019).

The present research work demonstrates the development of SMED methodology in the injection moulding process for the elimination of excessive time for mould changes to significantly increase productivity and decreasing monetary losses due to downtime due to changeover.

SMED (Single Minute Exchange of Dies)

Changeover time is generated in processes and is defined as the time between the last product that meets customer specifications and the first good product of the new production order (Ferradás & Salonitis, 2013). Several proposals have been developed to reduce these times, the most common is the methodology proposed by Shingeo Shingo called Single Minute Exchange of Die (SMED), which was designed as a technique for shop floor improvement focused on low-cost proposals based on Kaizen, later evolving to the Toyota production system (Jebaraj Benjamin et al., 2013; McIntosh et al., 2001). The SMED methodology according to its creator has four stages; process mapping, classifying activities as external or internal, transferring external and internal activities, streamlining external and internal activities (Rosa et al., 2017).

The sequence of assembly activities can be classified as internal and external with the aim that most activities are performed when the machine is in operation (external activities) in order to reduce the time the equipment is out of operation (Juarez-Vite et al., 2023; Moxham & Greatbanks, 2001).

SMED has been evaluated in several works where the advantages and improvements obtained with the implementation of the methodology are evaluated, in addition to obtaining information on the advantages and savings expected in the elimination of activities that do not add value to the products or processes (Almomani et al., 2013). SMED was initially limited only to manufacturing processes, nowadays, it is applied in various management services and assembly operations (Trovinger & Bohn, 2005).

Methodology

This research work was developed by choosing a qualitative approach because the aim is to collect information to be able to test a hypothesis based on a measurement that is subjected to statistical analysis.

The type of research presented is descriptive, because it seeks to describe the characteristics of a process, which serves for decision making and implementation of methodologies or tools that allow for improving the production process (Hernández Sampieri, Roberto / Fernández Collado, Carlos / Baptista Lucio, 2014).

The research design refers to the development of a work plan to collect the information required to answer the research question posed, this work is based on a descriptive design, since the collection and analysis of information is required to present the data collected for decision making in improving the injection process (Hernández Sampieri, Roberto / Fernández Collado, Carlos / Baptista Lucio, 2014). Mould changes in the injection moulding area are very recurrent due to the planned level of production as the week progresses and the requirements per project, changes have become a complex procedure involving staff training, tools, adjustment parameters and safety, which becomes a critical issue at the time of making approximately 20 changes per day in this area,

ISSN: 2410-3454

Without counting the changes that were not planned and that for some reason tend to be made from one moment to the next, therefore the response capacity of the assemblers, supervisors and managers of the area have to be optimal to make the change as quickly as possible, without affecting productivity at that time, without leaving aside the safety of personnel and physical assets that are included in that period. Structuring the above can be shown in the following diagram the phases to attack this condition and the tools and / or means that we will use, in Figure 1 shows the methodology proposed for the development of this research.

Figure 1 Methodology applied
Source: Own Elaboration

Development of the study

On the production floor, mainly in the injection moulding area, excessive time was observed when changing moulds on the injection moulding machines, which in the long run translates into large economic losses for the company, if we take into account the number of changes per day due to the time it takes to make a change either by waiting for the mould to reach the right temperature for assembly or by adding the number of SCRAP (defective parts).

The number of changes per week on each machine is shown below, with emphasis on the machine with the highest number of paths, as shown in figure 2.

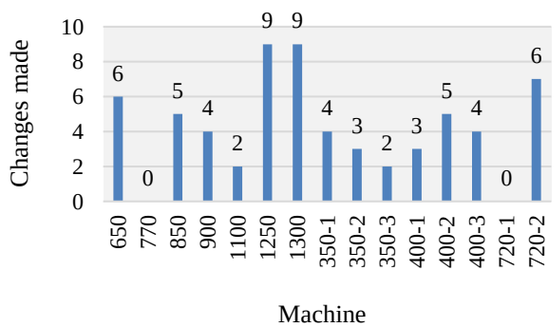

Figure 2 Change reporting
Source: Own Elaboration

Using as an example the 1250 machine for wood and the 720/2 for aluminium, the following figures are obtained, expressed in minutes and subsequently, the cost of having them on standby for an average time. Taking a minimum time of 145 minutes with respect to the activities carried out during the mould change considering the times established in the table 1.

Activity	Time (minutes)
Machinery shutdown	20
Transfer of moulds	20
Assembly to installation	80
Preparation and djustment	25
Total time	145

Table 1 Time study
Source: Own Elaboration

The above allows us to establish the production costs for products A and B that were subjected to analysis of the lost time generated by tooling changes. Table 2 shows the relevant calculations for two machines that process wood (A) and aluminium (B).

Weekly stoppages	
Product A	Product B
Equipment 1250	Equipment 720-2
9 (stoppages) x 145 min	6 (stoppages) x 145 min
1305 min = 21.75 hrs	870 min = 145.5 hrs

Table 2 Calculation of weekly stoppages
Source: Own Elaboration

How much does it cost us to make a change with a duration of 145 minutes (2:25 hrs) of between six and nine changes in two variants, (A and B) on two machines during one week, while the price of product A (wood) is € 2.36 and product B (aluminium) is € 2.77 using equation 1.

$$Costos = Piezas\ (hr) * Costo\ unitario \quad (1)$$

In one week for nine changes corresponding to machine 1250, where the runs were established for the parts of product A, we obtained 21.75 hours per mould change, taking into account that the minimum time was 145 minutes per change. From the above data, equation 1 can be developed to estimate the losses caused by tooling changes.

ISSN: 2410-3454

Having potential losses of between 3,213.2 and 4,517.04 euros per week, giving a total between these two parts of 7,730.24 euros in one week. This also generates problems of downtime, leading to bottlenecks and resulting in productivity problems and affecting other areas dependent on the injection moulding area.

The calculation of times was carried out by means of the study of times and movements, as such, we started by taking the cycle time of the machines and began to have an orderly record per machine in terms of its cycle time per machine, this also helped to obtain the production rates that later will help us to calculate the necessary times with respect to the time of preparation of the mould. As such, time study is defined as the procedure used to measure the time required by a skilled worker, working at a normal level of performance, to perform a given task according to a specified method, with due allowance for fatigue, personal delays and unavoidable delays (Maynard, 2006).

The four rules necessary for mould change were then implemented. The four Rules for performing a mould change are a set of requirements to ensure that the basis for a mould change is in place, thus tackling the bad habits that are taken when performing a change or adjustment, and they were established with the relevant process engineer to ensure that the procedure is performed as agreed.

Subsequently, we start with the process of calculating the parts per hour that are produced in an injection moulding machine, this calculation is developed from equation 2. The result of this equation is very important because only by knowing this information we will be able to know the most approximate time of completion of our current run. Knowing the end time of our production will allow us to properly prepare the mould to be assembled. Both assembler, materialist and operator will have a clear schedule and will be very attentive to perform their functions in a mould change.

$$Piezas\ x\ hora = \frac{3600}{TC*CAV} \quad (2)$$

Based on equation 1, calculations are made for products A and B where the injection cycle time of the aforementioned gates is, in the case of product A, 81 seconds and the mould has two injection cavities, which gives us two pieces per cycle.

In the case of product B, with a shorter cycle time of 45 seconds and with two cavities, we also obtain two pieces per cycle. Carrying out the operations, 3600 seconds equivalent to one hour are divided by the cycle time of the machine and multiplied by two in this case, the result will tell us the number of parts produced in one hour.

Results

In order to be able to compare the impact of the project, a first time measurement was carried out on the M1300, M1250, M1100 and M900 machines, the times for mould changes were obtained on these machines, the diagnosis of the production lines was started, and in figure 2 you can see the times that will be reduced.

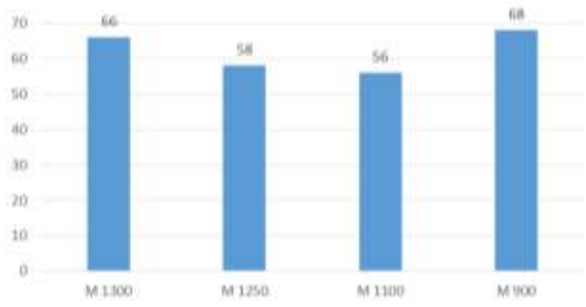

Figure 2 Initial mould change time
Source: Own Elaboration

The times obtained with respect to the minimum initial time condition (145 min) are shown in table 3.

Observation	Time
Initial condition	145 minutes
Test 1	53 minutes
Test 2	25 minutes
Final test	15 minutes

Table 3 Test times
Source: Own Elaboration

ISSN: 2410-3454

Based on these results, the annual cost for equipment preparation and non-productive hours, which directly affect the plant's productivity, was calculated. In the cost factor, the annual calculation was made taking as a reference the times obtained during the test and the period in which the first results were obtained. Taking as a reference the minimum value of the previous condition, changeover time for one hundred and forty-five minutes equivalent to two hours and twenty-five minutes compared with the result of the test runs (53, 25 and 15 minutes). In the case of product A, table 4 shows the results obtained in an initial condition prior to the implementation of the SMED methodology.

Initial condition	
Unit cost	€ 2.36
Weekly	€ 4, 5147.04
Monthly	€ 18, 068.08
Annual	€ 216,817.92

Table 4 Non-productive time costs
Source: Own Elaboration

The weekly, monthly and annual calculation was made based on the production rates, a calculation corresponding to the product of the number of pieces per week that are produced by the unit price of each piece, this initial condition having an annual cost of 216,817.92 euros. When carrying out the test runs to take the time that was reduced, it can be seen in table 5, in relation to the cost of these changes in the year. Obtaining savings of up to 90 % equivalent to 194, 388.48 euros.

Cost	Initial Condition	Test 1	Test 2
Unit cost	€ 2.36	€ 2.36	€ 2.36
Weekly	€1651.06	€ 778.80	€ 467.28
Monthly	€6604.22	€3115.20	€1869.12
Annual	€79250.6	€37382.4	€22429.4

Table 5 Cost reduction
Source: Own Elaboration

For the case of product B, the same was the case, here we could observe the variant of changes in the machine 720 / 2 corresponding to aluminium injection, since this one, presented a smaller number of changes per week, in table 6 the relevant calculations are observed where there is an obvious difference between unit cost and the ratio of changes per lapse.

Condición inicial	
Unit cost	€ 2.77
Weekly	€ 5, 301.78
Monthly	€ 21,207.12
Annual	€ 254,485.44

Table 6 Costs for non-productive times
Source: Own Elaboration

By performing the test runs to take the time that was reduced by applying the same calculations that were used for product A, now with the price of product B, the comparative results are shown in table 6.

Cost	Initial Condition	Test 1	Test 2
Unit cost	€ 2.77	€ 2.77	€ 2.77
Weekly	€ 1174.48	€ 554.00	€ 467.28
Monthly	€ 4697.92	€ 2216.0	€1869.12
Annual	€ 26375.0	€ 26592	€22429.4

Table 7 Cost reduction product B
Source: Own Elaboration

In this case the values were different as there was a variable with respect to the number of changes per week made by the machine where the part is run, this number corresponds to 6 changes per week, 3 less than the machine but without a doubt important figures were obtained at the end of the productive year. Obtaining a saving of over 93%, equivalent to 238,530.24 euros, the figure that we obtained by having carried out these three runs to be able to take the non-productive time and on this basis work on standardising the method.

The application of the SMED methodology is reflected in the medium term and reflects the success in mould change times. The initiatives that were implemented for the improvement of the processes took place gradually, the changeover time at the end of the project reduced the mould changeover times on various machines as shown in figure 3.

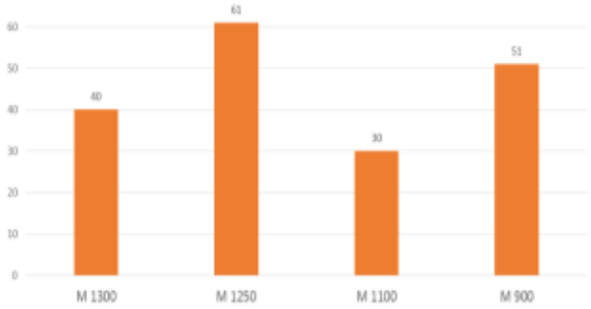

Figure 3 Final time reduction
Source: Own Elaboration

ISSN: 2410-3454

Conclusions

In summary, positive numbers were obtained with respect to the time per mould change, obtaining a record change time of 15 minutes, demonstrating that if we look for the appropriate conditions and the necessary tool we can have the minimum time as well as obtaining a maximum time of 3 hours; the causes for which these times were obtained are shown in the history, as well as the control of these changes.

This work was carried out in order to reduce the excessive time in the changes of injection moulds for both aluminium and wood, each of these in their respective pilot areas that were implemented in strategic points were of great help in detecting other areas of opportunity for injection in general.

The work was documented in relation to the design of a S.M.E.D. system in order to optimise times in the injection moulding area, specifically when making mould changes in the machines due to an unforeseen or planned change. This system will help us to achieve minimum times in the changes, with an elaborated and standardised method to also increase the productivity of the area, reducing losses due to tooling changes, dead times, eliminating bottlenecks without affecting the flow of the process and also the quality of the product.

References

Almomani, M. A., Aladeemy, M., Abdelhadi, A., & Mumani, A. (2013). A proposed approach for setup time reduction through integrating conventional SMED method with multiple criteria decision-making techniques. *Computers and Industrial Engineering*. https://doi.org/10.1016/j.cie.2013.07.011

da Silva, I. B., & Godinho Filho, M. (2019). Single-minute exchange of die (SMED): a state-of-the-art literature review. *International Journal of Advanced Manufacturing Technology*, *102*(9–12), 4289–4307. https://doi.org/10.1007/s00170-019-03484-w

Ferradás, P. G., & Salonitis, K. (2013). Improving changeover time: A tailored SMED approach for welding cells. *Procedia CIRP*. https://doi.org/10.1016/j.procir.2013.06.039

Hernández Sampieri, Roberto / Fernández Collado, Carlos / Baptista Lucio, Pilar. (2014). Metodología de la Investigación. In *McGRAW-HILL / INTERAMERICANA EDITORES, S.A. DE C.V.*

Jebaraj Benjamin, S., Murugaiah, U., & Srikamaladevi Marathamuthu, M. (2013). The use of SMED to eliminate small stops in a manufacturing firm. *Journal of Manufacturing Technology Management*. https://doi.org/10.1108/17410381311328016

Juárez-Vite, A., Corona-Armenta, J. R., Rivera-Gómez, H., Montaño-Arango, O., & Medina-Marín, J. (2023). Application of the SMED methodology through folding references for a bus manufacturing company. *International Journal of Industrial Engineering and Management*, *14*(3), 232–243. https://doi.org/10.24867/IJIEM-2023-3-335

Kemal Karasu, M., Cakmakci, M., Cakiroglu, M. B., Ayva, E., & Demirel-Ortabas, N. (2014). Improvement of changeover times via Taguchi empowered SMED/case study on injection molding production. *Measurement: Journal of the International Measurement Confederation*, *47*(1), 741–748. https://doi.org/10.1016/j.measurement.2013.09.035

Lozano, J., Saenz-Díez, J. C., Martínez, E., Jiménez, E., & Blanco, J. (2019). Centerline-SMED integration for machine changeovers improvement in food industry. *Production Planning and Control*. https://doi.org/10.1080/09537287.2019.1582110

McIntosh, R. I., Culley, S. J., Mileham, A. R., & Owen, G. W. (2001). Changeover improvement: A maintenance perspective. *International Journal of Production Economics*. https://doi.org/10.1016/S0925-5273(00)00170-5

Moxham, C., & Greatbanks, R. (2001). Prerequisites for the implementation of the SMED methodology: A study in a textile processing environment. *International Journal of Quality and Reliability Management*. https://doi.org/10.1108/02656710110386798

ISSN: 2410-3454

Pacheco, DADJ y Heidrich, GDG (2023). Revitalizar las actividades de reducción de setup en la Dirección de Operaciones. Planificación y control de la producción, 34 (9), 791-811.

Rosa, C., Silva, F. J. G., Ferreira, L. P., & Campilho, R. (2017). SMED methodology: The reduction of setup times for Steel Wire-Rope assembly lines in the automotive industry. *Procedia Manufacturing*. https://doi.org/10.1016/j.promfg.2017.09.110

Trovinger, S. C., & Bohn, R. E. (2005). Setup time reduction for electronics assembly: Combining simple (SMED) and IT-based methods. *Production and Operations Management*. https://doi.org/10.1111/j.1937-5956.2005.tb00019.x

ISSN: 2410-3454

Article **Journal of Engineering Applications**
June 2023 Vol.7 No.19 28-33

Determination of risk zones by thermal flow, generated by BLEVE to a tank with LP gas, using mathematical models and ALOHA® software

Determinación de zonas de riesgo por flujo térmico, generada por BLEVE a depósito con gas LP, utilizando modelos matemáticos y software ALOHA®

TORRES-VALLE, José Bernardo†, HERNÁNDEZ-BORJA, Carlos, PEZA-ORTÍZ, Edebaldo and PÉREZ-GALINDO, Liliana Eloisa

Universidad Tecnológica Fidel Velázquez - Mantenimiento Industrial y Mecatrónica

ID 1st Author: *José Bernardo, Torres-Valle* / **ORC ID**: 0000-0002-4302-1640

ID 1st Co-author: *Carlos, Hernández-Borja* / **ORC ID**: 0000-0002-8138-9016

ID 2nd Co-author: *Edebaldo, Peza-Ortíz* / **ORC ID**: 0000-0003-0236-883X

ID 3rd Co-author: *Liliana Eloisa, Pérez-Galindo* / **ORC ID**: 0000-0001-6016-2595

DOI: 10.35429/JEA.2023.29.10.28.33 Received: January 30, 2023; Accepted: June 30, 2023

Abstract

The objective of this research work was to determine the risk areas for thermal radiation, generated by BLEVE and fireball in a 13,000 L tank with LP gas, located in the municipality of Nicolás Romero, State of Mexico, from of mathematical models and the ALOHA® software, in order to compare and analyze the results obtained. In order to carry out the solution of this work, first the event and hypothetical scenario in which the type of applicable source was defined, which is BLEVE followed by fireball, is judged, and later different data were determined for the present study. Based on the above, the corresponding modeling was carried out to determine the risk zones of affectation by thermal radiation, the dimension of the diameter and the duration of the fireball. As a result, a comparative analysis was obtained in which it was possible to observe and conclude that the results obtained through mathematical models, in general, present more conservative results, compared to the modeling used by ALOHA®.

BLEVE, Fireball, Thermal Flux

Resumen

El objetivo del presente trabajo de investigación fue determinar las zonas de riesgo por radiación térmica, generada por BLEVE y bola de fuego (fireball) a depósito de 13,000 L con gas LP, ubicado en el municipio de Nicolas Romero, Estado de México, a partir de modelos matemáticos y el software ALOHA®, con el fin de comparar y analizar los resultados obtenidos. Para poder llevar a cabo la solución del presente trabajo, primero se determinó el evento y escenario hipotético en el cual se definió el tipo de fuente aplicable, que es BLEVE seguido por bola de fuego, y posteriormente se determinaron diferentes datos para el presente estudio. A partir de lo anterior, se realizaron los modelados correspondientes para la determinación de zonas de riesgo de afectación por radiación térmica, dimensión del diámetro y duración de la bola de fuego. Como resultado, se obtuvo un análisis comparativo en el cual se pudo observar y concluir, que los resultados obtenidos por medio de modelos matemáticos, de forma general, presentan resultados más conservadores, comparado con el modelado utilizado por ALOHA®.

BLEVE, Bola de fuego, Flujo térmico

Citation: TORRES-VALLE, José Bernardo, HERNÁNDEZ-BORJA, Carlos, PEZA-ORTÍZ, Edebaldo and PÉREZ-GALINDO, Liliana Eloisa . Determination of risk zones by thermal flow, generated by BLEVE to a tank with LP gas, using mathematical models and ALOHA® software. Journal of Engineering Applications. 2023. 10-29: 28-33

* Correspondence of the Author (e-mail: jose.torres@utfv.edu.mx)
† Researcher contributing as first author.

Introduction

LPG is a petroleum derivative composed of propane and butane gases. For ease of handling, it is converted to a liquid state through compression and cooling, from which it takes the name liquefied petroleum gas or LP gas (CENAPRED, 2019).

LPG has been used for industrial and domestic purposes since the beginning of the 20th century (CONUEE, 2015).

Liquefied Petroleum Gas can go into BLEVE (Boiling Liquid Vapour Expansion Explosion) within minutes, so the main hazards are: Fire, thermal radiation from fire, explosion and projectiles (PEMEX, 2015).

BLEVE are among the most feared events, when there are closed tanks of hazardous materials in liquid or gaseous state that are exposed to fire (Garza, 2015). It corresponds to a violent vaporisation of an explosive nature after rupture (loss of confinement) of a tank containing a liquid at a temperature significantly higher than its normal boiling point at atmospheric pressure (AIChE/CCPS, 2010).

In the case of flammable substances, BLEVE is often followed by a fireball (Salla, 2006). Moreover, the combined action of a BLEVE fireball can be summarised in the following effects (Casal, 2017):

– Thermal radiation
– Pressure wave
– Flying fragments

Likewise, in this document, the simulation of a possible thermal risk, hypothetical scenario, is determined for a storage tank of 13,000 L of LP Gas, located in the municipality of Nicolás Romero, State of Mexico.

The purpose of this simulation is that from a hypothetical scenario, a BLEVE and a fireball are produced, and from mathematical models and the ALOHA® software, a comparison of results is made, in which the areas and/or zones of affectation by thermal radiation are determined. These zones and

These zones and their respective radiation parameters are defined on the basis of the Civil Protection Technical Standard NTE-002- CGPC-2018. It is worth mentioning that the different zones mentioned correspond to the lethality zone, risk zone and buffer zone, corresponding to the risk of BLEVE due to the effect of thermal radiation.

Methodology

Hypothetical event

The event is considered in which the LPG tank, with a capacity of 13,000 L, is exposed to fire, due to the domino effect of another event.

Hypothetical scenario

Derived from this overheating, the substance enters the boiling liquid expansion phase, thus generating a violent explosion, denominating this BLEVE type effect which is followed by a fireball.

Collection of miscellaneous data for modelling

The various data and values needed to carry out the respective modelling are as follows:

a) Volume of the liquid (propane) = 13 m3
b) Density of liquid at 15°C = 510 kg/m3
c) Radiative fraction of heat of combustion = 46,354.854 kJ/kg
d) Partial vapour pressure of water = 785.517022 Pa
e) Relative humidity = 52%.
f) Ambient temperature = 285.65 K

Mathematical modelling

In order to carry out the mathematical modelling of the effect of BLEVE by thermal radiation, the following concepts were determined.

Physical parameters of BLEVE

Useful formulae for the physical parameters of BLEVE are (AIChE/CCPS, 2000):

Maximum fireball diameter D_{Max} (m):

$$D_{MAX} = 5.8\, M^{1/3} \quad (1)$$

ISSN: 2410-3454

Duration of fireball combustion t (s):

$t_{BLEVE} = 0.45\ M^{1/3}$ para M < 30,000 kg (2)

$t_{BLEVE} = 2.6\ M^{1/3}$ para M > 30,000 kg (3)

Where:

M = is the initial mass of the flammable liquid (kg).

Height of the centre of the fireball H_{BLEVE} (m):

$H_{BLEVE} = 0.75$ (4)

Heat radiation flux of the fireball BLEVE

Figure 1 shows the geometrical relationship (distance) from the centre of the fireball to the receiver; X_C (m).

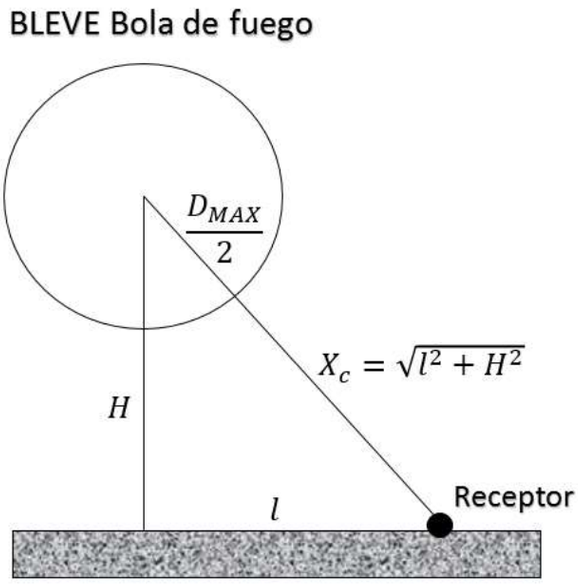

Figure 1 Geometry of the centre of the fireball at the receiver

In other words:

$X_c = \sqrt{l^2 + H^2}$ (5)

Where:

l: Distance from the point on the ground

Hymes (1983, as cited in Garza, 2015) gives an equation for estimating the heat flux to the surface, based on the radiant fraction of the total heat of combustion:

$E_r = \frac{2.2\tau_a R H_c M^{\frac{2}{3}}}{4\pi X_c^2}$ (6)

Where:

$\boldsymbol{E_r}$ = Radiant flux received by the receiver (W/m^2)
τ_a = Atmospheric transmissivity (unitless)
R = Radiant fraction of heat of combustion (without units)
H_c= Net heat of combustion per unit mass (J/kg)
M = Initial mass of fuel in the fireball (kg)

The atmospheric transmissivity can be expressed from the following equation (CCPS, 2000):

$\tau_a = 2.02\left[P_w((H^2 + l^2)^{\frac{1}{2}} - \frac{D_{MAX}}{2})\right]^{-0.09}$ (7)

Where:

τ_a = Atmospheric transmissivity (unitless)
P_w = Partial pressure of water (Pascals, N/m2)
H = Height of the center of the fireball H (m)
l = Distance from point on the ground, directly below the center of the fireball, to the receiver

Mudan and Croce (1988, as cited in AIChE/CCPS, 2000) give an expression for the partial pressure of water as a function of relative humidity and air temperature:

$P_w = 1013.25(R_H)exp\left(14.4114 - \frac{5328}{T_a}\right)$ (8)

Where:
P_w = Partial pressure of water (Pascals, N/m^2)
R_H = relative humidity (%)
T_a = Room temperature (K)

Modelling the event using ALOHA

The ALOHA® software was used to simulate the hypothetical scenario of interest, based on the determination of the thermal radiation risk zones. To carry out the simulation, the methodology used to obtain the results consisted first of establishing the location of the site where the LP Gas tank was located, this location was taken as a reference in the municipality of Nicolás Romero, State of Mexico, then the substance to be analysed was determined, in this case propane was considered as the substance with the greatest presence in the LP Gas.

ISSN: 2410-3454

Likewise, the atmospheric data of the place was determined, as well as the dimensional characteristics of the tank, among others. Finally, it was established in ALOHA® that the type of event generated was a BLEVE. It is worth mentioning that the tank was considered to contain only liquid due to the storage pressure and temperature conditions.

Based on the above, the results of the radii and/or zones affected were obtained in the ALOHA® program, and these were linked to the Google Earth® software, in order to obtain these radii on a georeferenced aerial map and compare these results with those obtained from the mathematical modelling mentioned above.

Results

In order to determine the results, both for the mathematical modelling and for the modelling using ALOHA, different values of thermal radiation limits and their respective zones have been considered. These values and zones are based on the CIVIL PROTECTION TECHNICAL STANDARD NTE-002-CGPC-2018. It should be noted that, for the present modelling, the tank has been estimated with LPG at 80% of its maximum capacity.

Results obtained using mathematical models

By simulating the heat flux (thermal radiation) risk scenario, different parameters related to the BLEVE risk have been obtained.

Table 1 below shows the parameters and results obtained for the BLEVE fireball.

Thermal radiation zone	Radiation limit Er (kW/m2)	Distance to receiver XC (m)	Maximum fireball diameter D_{MAX} (m)	Duration of the fireball tBLEVE (s)	Height of the fireball HBLEVE (m)
Lethality zone	10.00	241.45	108.96	8.45	81.72
Risk area	5.0	336.38	108.96	8.45	81.72
Buffer zone	1.4	618.62	108.96	8.45	81.72

Table 1 BLEVE Fireball Parameters

From the results obtained for the three different heat flux risk zones; lethality zone (10 kW/m2), risk zone (5 kW/m2) and buffer zone (1.4 kW/m2), respectively, in the following Figure 2, the relationship of the distance from the centre of the fireball to the receiver is graphically represented, observing that as the distance from the receiver to the centre of the fireball increases, the heat flux (radiation) decreases, i.e., it decreases.

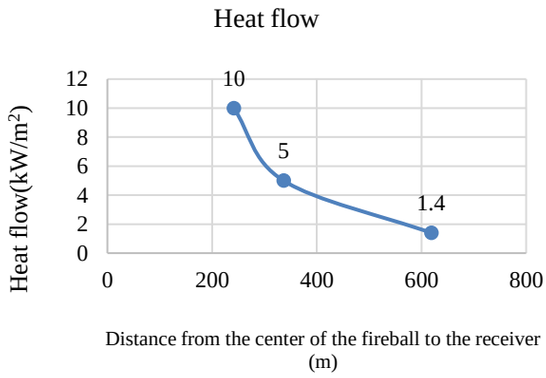

Figure 2 Heat flux radiated by the explosion of the LPG container at different distances from the source of the explosion

Results of modelling the event using ALOHA

Diameter, duration and threat zones of the fireball

Figure 3 below shows the results for the diameter, duration and threat zones of the fireball. ALOHA® automatically determines these results by providing information related to the atmospheric conditions at the event site, physico-chemical properties of the substance involved and dimensional data of the deposit, primarily.

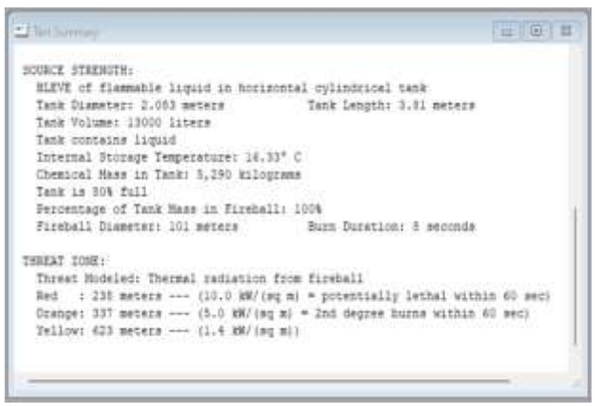

Figure 3 Results of the radii and/or thermal radiation threat zones for the LP-Gas explosion in a BLEVE.

Thermal Radiation Threat Zones

The thermal radiation threat zone due to the BLEVE explosion of the 13,000 L LP gas tank can be seen in Figure 4 below.

ISSN: 2410-3454

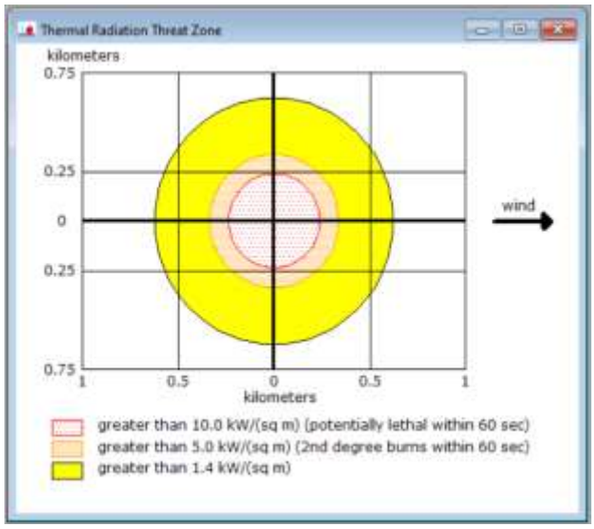

Figure 4 Threat zones due to thermal radiation from the LP gas explosion

From the results obtained, these are transferred to Google Earth® in order to identify the site of the LP gas tank on a cartographic level, as well as the respective threat zones already mentioned. This information can be seen in Figure 5 below.

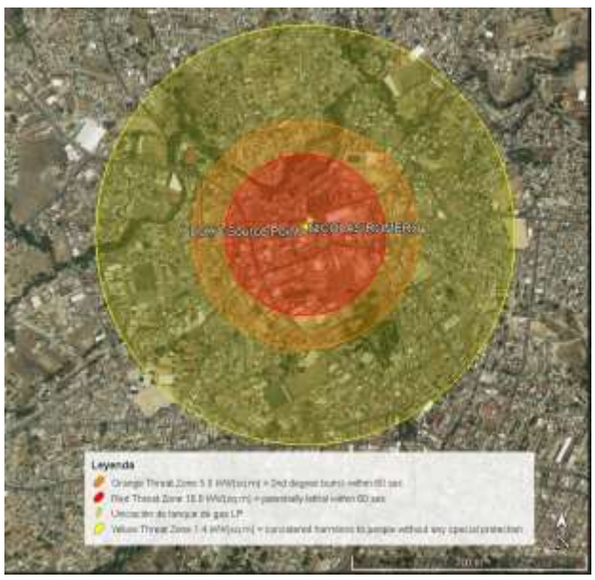

Figure 5 Cartographic representation of thermal radiation hazard areas

It is worth mentioning that the results obtained with ALOHA® show that from the site of the explosion and up to a distance of 238 m, it would be determined as a lethal zone and would experience thermal radiation that could cause death; between a distance of 238 m to 337m corresponds to a risk zone and second degree burns would be experienced in 60 seconds of exposure.

And between 337 m and 623m would correspond to a buffer zone in which this zone is considered harmless for people without any special protection.

Comparative analysis of the results obtained

Based on the results obtained, both from the use of mathematical models and from the use of ALOHA®, Table 2 below shows the results for the zones of risk and/or affectation by thermal radiation, as well as the respective percentage difference between them.

Thermal radiation zone	Radiation limit E_r (kW/m2)	Models Mathematicians Distance to receiverX_C (m)	Models Mathematicians Distance to receiverXC (m)	Difference between models used (%)
Lethality zone	10.00	241.45	238	1.428
Risk area	5.0	336.38	337	0.184
Buffer zone	1.4	618.62	623	0.703

Table 2 Comparative results of thermal radiation risk zones

Likewise, the following Table 3 presents a comparison of the results obtained, corresponding to the diameter and duration of the fireball.

Parameter	Models Mathematics	Modelling in ALOHA ®	Difference between models used (%)
Diameter maximum fireball diameter D_MAX (m)	108.96	101	7.305
Duration of fireball BLEVE (s)	8.45	8	5.325

Table 3 Comparison of results of diameter and duration of the fireball

Acknowledgements

We are grateful for the support provided by the Universidad Tecnológica Fidel Velázquez for this work.

Funding

Funding: The following work is not supported by any type of funding.

Conclusions

The following conclusions can be drawn from this research:

ISSN: 2410-3454

The results obtained to determine the thermal radiation risk zones, with respect to the comparison of mathematical models and modelling with ALOHA®, as can be seen in Table 2, show that the lethality zone presents the highest percentage difference between these models, with a value of 1.428%. Likewise, the widest value of this lethality zone is presented by the application of the mathematical modelling, considering a more conservative result for this zone. Likewise, for the case of the risk zone and buffer zone, the percentage difference is 0.184% and 0.703%, respectively, which represents a minimum percentage between them. It is worth mentioning that, for the comparison with respect to the results of the diameter and duration of the fireball, presented in Table 3, the percentage difference of the applied modelling corresponds to 7.305% and 5.325%, respectively. It can be seen that the highest values obtained for both the diameter and the duration of the fireball are obtained from the mathematical modelling. Likewise, it can be concluded, in general, that the results obtained from the use of mathematical models present the most conservative values of the present work carried out.

On the other hand, the use of modelling from the ALOHA® software for the present research work is simpler to carry out, as well as illustrative, since it allows the linkage with other programs, such as Google Earth®, in which the different areas of risk due to thermal radiation can be visualised at satellite image level, based on the study site.

It is worth mentioning that LP gas is a fuel that is in great demand for use in industries, shops, restaurants, homes, vehicles, etc. and it is vitally important to consider regulatory aspects for its transport and storage, given that it is highly flammable and can generate a risk of explosion if it leaks and accumulates in a closed and/or confined space.

References

AIChE/CCPS. (2000). *Guidelines for chemical Process Cuantitative Risk Analysis.* (S. E. ed., Ed.) New York, USA: Wiley Interscience.

AIChE/CCPS. (2010). *Guidelines for Vapor Cloud Explosion, Pressure Vessel Burst, BLEVE, and Flash Fire Hazards* (2nd Edition ed.). NJ, USA: Wiley-Interscience.

Casal, J. (2017). *Evaluation of the Effects and Consequences of Major Accidents in Industrial Plants* (Second ed.). ELSEVIER.

CENAPRED (2019). (2023, agosto 14). *Gas LP*. Retrieved from https://www.cenapred.unam.mx/es/Publicaciones/archivos/290-INFOGRAFAGASLP.PDF

CGPC. (2018). *Norma Técnica de Protección Civil NTE-002-CGPC-2018, Que establece los lineamientos y las especificaciones para la elaboración del análisis de vulnerabilidad y riesgo de protección civil.* Coordinación General de Protección Civil, Gaceta del Gobierno, miércoles 25 de julio de 2018.

CONUEE (Comisión Nacional para el Uso Eficiente de la Energía) (2015). (2023, agosto 15). *Gas Licuado del Petróleo*. Retrieved from https://www.gob.mx/cms/uploads/attachment/file/94616/gasLP.pdf

Garza Ayala, S. (2015). *Análisis de Riesgos/Peligros en los Procesos.* México: Dinámica Euristica.

Hymes, I. (1983). *SRD R275: The Physiological and Pathological Effects of Thermal Radiation".* Culcheth, UK: UK Atomic Energy Authority.

J. M. Salla, M. D. (2006). BLEVE: A new approach to the superheat limit temperature. *Journal of Loss Prevention in the Process Industries*, 690-700.

PEMEX (2015). (2023, agosto 3). *Hoja de datos de seguridad; Gas Licuado del Petróleo*. Retrieved from https://www.pemex.com/comercializacion/productos/HDS/gas/HDS%20SAC%20%20Gas%20licuado%20del%20petr%C3%B3leo%20TRI-11%20v1.1.pdf

ISSN: 2410-3454

[Title in Times New Roman and Bold No. 14 in English and Spanish]

Surname (IN UPPERCASE), Name 1st Author†*, Surname (IN UPPERCASE), Name 1st Coauthor, Surname (IN UPPERCASE), Name 2nd Coauthor and Surname (IN UPPERCASE), Name 3rd Coauthor

Institutional Affiliation of Author including Dependency (No.10 Times New Roman and Italic)

International Identification of Science - Technology and Innovation

ID 1st Author: (ORC ID - Researcher ID Thomson, arXiv Author ID - PubMed Author ID - Open ID) and CVU 1st author: (Scholar-PNPC or SNI-CONACYT) (No.10 Times New Roman)

ID 1st Coauthor: (ORC ID - Researcher ID Thomson, arXiv Author ID - PubMed Author ID - Open ID) and CVU 1st coauthor: (Scholar or SNI) (No.10 Times New Roman)

ID 2nd Coauthor: (ORC ID - Researcher ID Thomson, arXiv Author ID - PubMed Author ID - Open ID) and CVU 2nd coauthor: (Scholar or SNI) (No.10 Times New Roman)

ID 3rd Coauthor: (ORC ID - Researcher ID Thomson, arXiv Author ID - PubMed Author ID - Open ID) and CVU 3rd coauthor: (Scholar or SNI) (No.10 Times New Roman)

(Report Submission Date: Month, Day, and Year); Accepted (Insert date of Acceptance: Use Only ECORFAN)

Abstract (In English, 150-200 words)

Objectives
Methodology
Contribution

Abstract (In Spanish, 150-200 words)

Objectives
Methodology
Contribution

Keywords (In English)

Indicate 3 keywords in Times New Roman and Bold No. 10

Keywords (In Spanish)

4Indicate 3 keywords in Times New Roman and Bold No. 10

Citation: Surname (IN UPPERCASE), Name 1st Author, Surname (IN UPPERCASE), Name 1st Co-author, Surname (IN UPPERCASE), Name 2nd Co-author and Surname (IN UPPERCASE), Name 3rd Co-author. Paper Title. Journal of Engineering Applications. Year 1-1: 1-11 [Times New Roman No.10]

* Correspondence to Author (example@example.org)
† Researcher contributing as first author.

Introduction

Text in Times New Roman No.12, single space.

General explanation of the subject and explain why it is important.

What is your added value with respect to other techniques?

Clearly focus each of its features

Clearly explain the problem to be solved and the central hypothesis.

Explanation of sections Article.

Development of headings and subheadings of the article with subsequent numbers

[Title No.12 in Times New Roman, single spaced and bold]

Products in development No.12 Times New Roman, single spaced.

Including graphs, figures and tables-Editable

In the article content any graphic, table and figure should be editable formats that can change size, type and number of letter, for the purposes of edition, these must be high quality, not pixelated and should be noticeable even reducing image scale.

[Indicating the title at the bottom with No.10 and Times New Roman Bold]

4

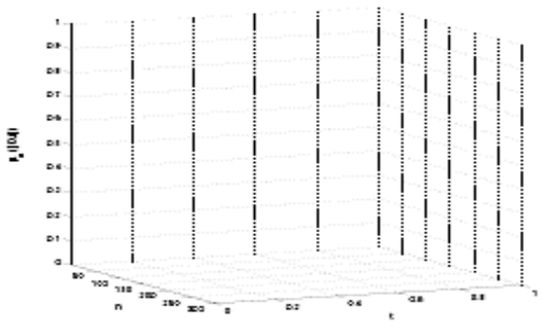

Graphic 1 Title and *Source (in italics)*

Should not be images-everything must be editable.

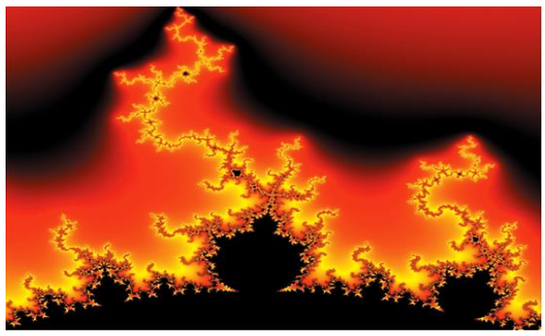

Figure 1 Title and *Source (in italics)*

Should not be images-everything must be editable.

Table 1 Title and *Source (in italics)*

Should not be images-everything must be editable.

Each article shall present separately in **3 folders**: a) Figures, b) Charts and c) Tables in .JPG format, indicating the number and sequential Bold Title.

For the use of equations, noted as follows:

$$Y_{ij} = \alpha + \sum_{h=1}^{r} \beta_h X_{hij} + u_j + e_{ij} \qquad (1)$$

Must be editable and number aligned on the right side.

Methodology

Develop give the meaning of the variables in linear writing and important is the comparison of the used criteria.

Results

The results shall be by section of the article.

Annexes

Tables and adequate sources

Thanks

Indicate if they were financed by any institution, University or company.

Conclusions

Explain clearly the results and possibilities of improvement.

ISSN 2410-3454

References

Use APA system. Should not be numbered, nor with bullets, however if necessary numbering will be because reference or mention is made somewhere in the Article.

Use Roman Alphabet, all references you have used must be in the Roman Alphabet, even if you have quoted an Article, book in any of the official languages of the United Nations (English, French, German, Chinese, Russian, Portuguese, Italian, Spanish, Arabic), you must write the reference in Roman script and not in any of the official languages.

Technical Specifications

Each article must submit your dates into a Word document (.docx):

Journal Name
Article title
Abstract
Keywords
Article sections, for example:

1. Introduction
2. Description of the method
3. Analysis from the regression demand curve
4. Results
5. Thanks
6. Conclusions
7. References

Author Name (s)
Email Correspondence to Author
References

Intellectual Property Requirements for editing:

- Authentic Signature in Color of Originality Format Author and Co-authors
- Authentic Signature in Color of the Acceptance Format of Author and Co-authors
- Authentic Signature in blue Color of the Conflict of Interest Format of Author and Co-authors.

ISSN 2410-3454

Reservation to Editorial Policy

Journal of Engineering Applications reserves the right to make editorial changes required to adapt the Articles to the Editorial Policy of the Journal. Once the Article is accepted in its final version, the Journal will send the author the proofs for review. ECORFAN® will only accept the correction of errata and errors or omissions arising from the editing process of the Journal, reserving in full the copyrights and content dissemination. No deletions, substitutions or additions that alter the formation of the Article will be accepted.

Code of Ethics - Good Practices and Declaration of Solution to Editorial Conflicts

Declaration of Originality and unpublished character of the Article, of Authors, on the obtaining of data and interpretation of results, Acknowledgments, Conflict of interests, Assignment of rights and Distribution

The ECORFAN-Mexico, S.C Management claims to Authors of Articles that its content must be original, unpublished and of Scientific, Technological and Innovation content to be submitted for evaluation.

The Authors signing the Article must be the same that have contributed to its conception, realization and development, as well as obtaining the data, interpreting the results, drafting and reviewing it. The Corresponding Author of the proposed Article will request the form that follows.

Article title:

– The sending of an Article to Journal of Engineering Applications emanates the commitment of the author not to submit it simultaneously to the consideration of other series publications for it must complement the Format of Originality for its Article, unless it is rejected by the Arbitration Committee, it may be withdrawn.

– None of the data presented in this article has been plagiarized or invented. The original data are clearly distinguished from those already published. And it is known of the test in PLAGSCAN if a level of plagiarism is detected Positive will not proceed to arbitrate.

– References are cited on which the information contained in the Article is based, as well as theories and data from other previously published Articles.

– The authors sign the Format of Authorization for their Article to be disseminated by means that ECORFAN-Mexico, S.C. In its Holding Bolivia considers pertinent for disclosure and diffusion of its Article its Rights of Work.

– Consent has been obtained from those who have contributed unpublished data obtained through verbal or written communication, and such communication and Authorship are adequately identified.

– The Author and Co-Authors who sign this work have participated in its planning, design and execution, as well as in the interpretation of the results. They also critically reviewed the paper, approved its final version and agreed with its publication.

– No signature responsible for the work has been omitted and the criteria of Scientific Authorization are satisfied.

– The results of this Article have been interpreted objectively. Any results contrary to the point of view of those who sign are exposed and discussed in the Article.

Copyright and Access

The publication of this Article supposes the transfer of the copyright to ECORFAN-Mexico, SC in its Holding Bolivia for it Journal of Engineering Applications, which reserves the right to distribute on the Web the published version of the Article and the making available of the Article in This format supposes for its Authors the fulfilment of what is established in the Law of Science and Technology of the United Mexican States, regarding the obligation to allow access to the results of Scientific Research.

Article Title:

Name and Surnames of the Contact Author and the Co-authors	Signature
1.	
2.	
3.	
4.	

Principles of Ethics and Declaration of Solution to Editorial Conflicts

Editor Responsibilities

The Publisher undertakes to guarantee the confidentiality of the evaluation process, it may not disclose to the Arbitrators the identity of the Authors, nor may it reveal the identity of the Arbitrators at any time.

The Editor assumes the responsibility to properly inform the Author of the stage of the editorial process in which the text is sent, as well as the resolutions of Double-Blind Review.

The Editor should evaluate manuscripts and their intellectual content without distinction of race, gender, sexual orientation, religious beliefs, ethnicity, nationality, or the political philosophy of the Authors.

The Editor and his editing team of ECORFAN® Holdings will not disclose any information about Articles submitted to anyone other than the corresponding Author.

The Editor should make fair and impartial decisions and ensure a fair Double-Blind Review.

Responsibilities of the Editorial Board

The description of the peer review processes is made known by the Editorial Board in order that the Authors know what the evaluation criteria are and will always be willing to justify any controversy in the evaluation process. In case of Plagiarism Detection to the Article the Committee notifies the Authors for Violation to the Right of Scientific, Technological and Innovation Authorization.

Responsibilities of the Arbitration Committee

The Arbitrators undertake to notify about any unethical conduct by the Authors and to indicate all the information that may be reason to reject the publication of the Articles. In addition, they must undertake to keep confidential information related to the Articles they evaluate.

Any manuscript received for your arbitration must be treated as confidential, should not be displayed or discussed with other experts, except with the permission of the Editor.

The Arbitrators must be conducted objectively, any personal criticism of the Author is inappropriate.

The Arbitrators must express their points of view with clarity and with valid arguments that contribute to the Scientific, Technological and Innovation of the Author.

The Arbitrators should not evaluate manuscripts in which they have conflicts of interest and have been notified to the Editor before submitting the Article for Double-Blind Review.

Responsibilities of the Authors

Authors must guarantee that their articles are the product of their original work and that the data has been obtained ethically.

Authors must ensure that they have not been previously published or that they are not considered in another serial publication.

Authors must strictly follow the rules for the publication of Defined Articles by the Editorial Board.

The authors have requested that the text in all its forms be an unethical editorial behavior and is unacceptable, consequently, any manuscript that incurs in plagiarism is eliminated and not considered for publication.

Authors should cite publications that have been influential in the nature of the Article submitted to arbitration.

Information services

Indexation - Bases and Repositories

LATINDEX (Scientific Journals of Latin America, Spain and Portugal)
RESEARCH GATE (Germany)
GOOGLE SCHOLAR (Citation indices-Google)
REDIB (Ibero-American Network of Innovation and Scientific Knowledge- CSIC)
MENDELEY (Bibliographic References Manager)
DULCINEA (Spanish scientific journals)
UNIVERSIA (University Library-Madrid)
SHERPA (University of Nottingham-England)

Publishing Services

Citation and Index Identification H
Management of Originality Format and Authorization
Testing Article with PLAGSCAN
Article Evaluation
Certificate of Double-Blind Review
Article Edition
Web layout
Indexing and Repository
ArticleTranslation
Article Publication
Certificate of Article
Service Billing

Editorial Policy and Management

21 Santa Lucía, CP-5220. Libertadores -Sucre – Bolivia. Phones: +52 1 55 6159 2296, +52 1 55 1260 0355, +52 1 55 6034 9181; Email: contact@ecorfan.org www.ecorfan.org

Journal of Engineering Applications

2410 3454
ISSN 2410 - 3454